Reviews

Epitaxial Stabilization of Oxides in Thin Films

O. Yu. Gorbenko,* S. V. Samoilenkov,† I. E. Graboy, and A. R. Kaul

Chemistry Department, Moscow State University, 119899 Moscow, Russia

Received January 14, 2002. Revised Manuscript Received April 19, 2002

A survey of recent experimental results is given, presenting the growth of oxide epitaxial thin films in $P-T-x$ conditions, which are far from those necessary for the existence of corresponding phases in a bulk state. The unstable in bulk $BaCu_3O_4$, $NdMn_7O_{12}$, $RNiO_3$, and unusual polymorphous forms of $BaRuO_3$, $RMnO_3$, TiO_2, and Mn_3O_4 are some examples. The stabilizing effect is observed only if epitaxial growth is induced. A rich variety of the effect observations are demonstrated to be of a thermodynamic origin, rather than of a kinetic one. Epitaxial stabilization is shown to be the result of the low energy of coherent interfaces formed due to epitaxy.

I. Introduction

Epitaxial growth of thin films has been intensively studied over more than half a century. Impressing progress has been made both in the theoretical understanding of epitaxy and in the growth of epitaxial films for applications.

The structural and dimensional resemblance between the film and the substrate often leads to a formation of coherent or semicoherent interfaces. The energy of coherent and semicoherent interfaces is significantly lower than that of noncoherent ones[1] (Table 1). In this way, the interface formed can affect the choice of the nucleus crystallographic structure because the system tends to minimize its free energy to reach the equilibrium state. The phenomenon is often referred to as "epitaxial stabilization", in case composition or crystallographic structure realized in the epitaxial film is different from that of the equilibrium bulk material. From a thermodynamic point of view, epitaxial stabilization demands the change of equilibrium phase diagrams due to epitaxial growth: in particular, the change of $P-T$ diagrams (epitaxial stabilization of metastable polymorphs) or $P-x$ and $T-x$ diagrams (epitaxial stabilization of metastable solid solutions and compounds with unusual stoichiometry).

That the formation of low-energy interfaces might cause stabilization of otherwise unstable (metastable, nonequilibrium) compounds or polymorphs has been known for a long time. The phenomenon has been documented by Dankov as early as the late 1930s.[2,3] It has been found that FeO with the structure allied to that of metallic Fe was formed as an epitaxial surface oxidation layer under $p(O_2)-T$ conditions, which did not correspond to the stability field of FeO in bulk. In 1951, Pashley[4] has reported the epitaxial growth of TlCl with a NaCl structure on a KBr substrate, while on NaCl, MgO, and mica substrates the normal CsCl-type structure of TlCl was observed. The result was explained by the lower lattice mismatch between KBr and an abnormal TlCl structure (6%), as compared to that with the normal one (17%).

Table 1. Ranges of Solid−Solid Interface Energies σ^{ss} for Three Types of Planar Interfaces[1]

interface	σ^{ss} (mJ/m^2)
coherent	5−200
semicoherent	200−800
incoherent	800−2500

Let us discuss the nature of this phenomenon in more detail. The phase stability is determined by both thermodynamic and kinetic factors, leading to equilibrium (thermodynamically stable) or metastable (stabilized due to kinetic reasons) states. Both cases can take place in epitaxial growth.

If the growth is performed under conditions of sufficient surface diffusion (enabling the growth of oriented crystalline phase), but low bulk diffusion (prohibiting phase transformations), the quenched metastable epitaxial structures can be obtained on single-crystalline substrates. This stabilization occurs evidently due to kinetic reasons.

The kinetic epitaxial stabilization of the vacuum-deposited materials was a subject of theoretical and experimental research for a long time. Thus, thin film synthesis of numerous solid solutions or polymorphous forms, which are metastable in the bulk state, has been reported: $(GaAs)_{1-x}Si_{2x}$, $(GaSb)_{1-x}Ge_{2x}$, $(GaAs)_{1-x}Ge_{2x}$, $Pb_{1-x}Cd_xS$, $InSb_{1-x}Bi_x$, $Ge_{1-x}Sn_x$, α-Sn, and $Ba_xCa_{1-x}F_2$.[5−9] These relatively thick (up to a few micrometers) epitaxial films have been obtained in a temperature window determined by surface and bulk diffusion coef-

* To whom correspondence should be addressed. E-mail: gorbenko@inorg.chem.msu.ru.
† Present address: IOPW, TU Braunschweig, Bienroder Weg 53, 38108 Braunschweig, Germany.

10.1021/cm021111v CCC: $22.00
Published on Web 09/07/2002

ficients. At temperature below the low-T limit, amorphous material was formed, while above the high-T limit the formation of equilibrium products was observed. The theoretical analysis of this phenomenon was given by Flynn and Yang.[10−12]

On the other hand, the "theory of pseudomorphism" has been proposed by Jesser,[13] in which the driving force for stabilization was the lowering of the interface energy due to coherency. In this case, the stabilization effect appears, owing to thermodynamic reasons of minimization of the systems free energy. The thermodynamic stability of epitaxial films has been addressed in more detail in studies on $(III-V)_{1-x}IV_{2x}$ semiconductors and other compounds in the 1970s and 1980s.

In the late 1970s Quillec et al.[14] achieved the growth of micrometer-thick epitaxial films of $In_{1-x}Ga_xAs_{1-y}P_y$ and $GaAs_{1-x}Sb_x$ solid solutions inside the immiscibility gap region on a InP substrate using liquid-phase epitaxy (LPE). Since LPE provides very fast mass transfer and low supersaturation, it is a process very close to equilibrium. Evidently, in this case any significant kinetic barriers are absent and the stabilization can take place exclusively due to the low energy of coherent interfaces formed.

In 1972, the drastic lattice mismatch influence on the composition of $Ga_{1-x}In_xP$ epitaxial layers grown by LPE on GaAs has been observed by Stringfellow[15] and Hirth and Stringfellow.[16] It has been reported that the growing film adopted nonequilibrium composition to minimize lattice mismatch with the substrate. This effect, referred to as a "composition pulling" or "latching effect", has much in common with the thermodynamic epitaxial stabilization.

Numerous evidences for the epitaxial stabilization of otherwise unstable compounds or polymorphous forms appeared in recent years as well: bcc-$Ni_{0.3}Fe_{0.7}$,[17] hcp- and bcc-Cu and Pd,[18] GaN with zinc blend,[19] cubic[20] and wurtzite structure,[21−23] cubic nitrides AlN,[24−26] TaN,[27] $CrN_{0.6}$,[28] and (Cd,Zn)S with wurtzite[29] and sphalerite structure.[30]

Profound thermodynamical analysis of epitaxy of otherwise unstable compounds was provided in the 1980−90s by Zangwill and co-workers[31−33] and Zunger and Wood.[34−36] The analysis proposed by Zunger with co-worker implies that all the constituents grow epitaxially in a strained state, until the misfit dislocations begin to nucleate at some critical thickness. Therefore, the phases with a large lattice mismatch to the substrate become less stable because of significant elastic strains applied. The theory explains the influence of the epitaxial growth of strained material on the equilibrium phase diagram. This approach works well only for systems where all the phases under consideration possess only a small lattice mismatch with a substrate, which is often the case for semiconducting solid solutions or metal alloys. Nevertheless, the approach fails to explain the epitaxial stabilization in film/substrate systems, where the strain is relieved through the formation of misfit dislocations.

A more general approach, which separates the structural incommensurability and the lattice strain at interfaces, was developed by Little and Zangwill.[37] To describe incommensurate interfaces, the Frenkel−Kontorova model was applied. In the frame of this theory, the formation of the phase with a coherent interface at low film thickness takes place due to the gain in the interface energy part related to commensurability. The lattice mismatch between the film and the substrate introduces the strain energy, which suppresses the epitaxial stabilization. At the critical thickness, which in the frame of this theory is expected to be comparable to 1-mL thickness, this contribution is balanced by the difference in volume free energies of the epitaxially stabilized compound and of the stable compound in bulk.

Roitburd[38] was the first one to point out the possibility of drastic reduction of the strain energy by the formation of so-called "periodic multiple-domain structures", expanding thus the epitaxial stabilization field significantly. The Little and Zangwill theory was combined with the Roitburd scenario in ref 31, producing sophisticated phase diagrams including epitaxial stabilization fields. The important conclusion in this work is that the transformation from an epitaxially stabilized phase to the equilibrium in the bulk phase does not appear abruptly, but rather covers the extended thickness range above the critical value. In this range both "metastable" and "stable" phases can grow simultaneously.

So it can be concluded that epitaxial stabilization—regarded as a thermodynamic phenomenon—increases with (a) the decrease of the free energy difference between "metastable" and "stable" phases in bulk, (b) the decrease of the film thickness, (c) the increase of the crystal structure coherency between the growing phase and the substrate, (d) the decrease of the shear and elastic moduli of the growing material, and (e) the ability of the growing material to form a periodic multiple-domain structure.

In the last 2 decades the growth of epitaxial oxide films is becoming increasingly more important. The materials of interest are high T_c superconductors, ferroelectrics, manganites with colossal magnetoresistance, various magnetic oxides, solid electrolytes, wide band-gap luminescent materials, and others.

Thus, a wide scope of experimental material has been reported on MBE growth of metastable superconducting cuprates and superlattices (see Bozovic and Eckstein,[39] Verbist et al.,[40] Balestrino et al.,[41] and Yamamoto et al.[42]—to name only a few). In this case, the growth is performed well below 600−700 °C and the stabilization effect is mainly due to kinetic reasons. At the same time, Raveau with co-workers[43] have reviewed the epitaxial growth of unstable in bulk complex oxides at higher temperature by common deposition techniques such as pulsed laser deposition (PLD). Unfortunately, no definite conclusions have been made in this work concerning the reasons for the stabilization phenomenon observed. Nevertheless, it is clear that epitaxial stabilization of oxides can be due to both thermodynamics and kinetics, as described above, and the general rules formulated for semiconductors and alloys must be applicable also to oxides.

There are some indications that the epitaxial stabilization due to thermodynamic reasons is highly possible in oxides. For example, the free energy of polymorphous transformations or solid-state reactions for many oxide systems is rather moderate. Also, the deviations from high symmetry are quite common in oxides, so the strain

energy can be easily reduced by the formation of periodic multiple-domain structures. All this means that the growth can often be performed at high temperature by common deposition techniques, resulting in films of high epitaxial quality. Also, in many cases the growth of epitaxially stabilized phases is possible up to the thickness, which might be important for applications.

In this review, high-temperature deposition experiments in systems with sufficient diffusion mobility are mainly considered to address epitaxial stabilization due to thermodynamic reasons. Critical analysis of recent publications on the subject is presented and some thermodynamic issues of this intriguing phenomenon are discussed. We intentionally do not consider the growth of ultrathin films (for example, 5-mL-thick (110)-VO_2/(110)TiO_2 [44] and 2-mL-thick (111)FeO/(0001)Al_2O_3 [45]) or stabilization effects caused by the surface energy of highly dispersed materials (e.g., the formation of polycrystalline γ-Al_2O_3 from amorphous alumina deposits[46]).

II. Epitaxial Stabilization of Polymorphous Forms

There are many examples of the epitaxial stabilization of different polymorphs of simple and complex oxides. It claims itself in epitaxial growth of different polymorphs on properly chosen substrates under the same $P-T$ conditions. The thermodynamic functions of many of these oxides are well-established, which may help in estimating the energy characteristics of the phenomenon.

IIa. Simple Metal Oxides. *A. TiO_2.* Rutile (space group $P4_2/mnm$, $a = 0.45933$ nm, $c = 0.29592$ nm) and anatase (space group $I4_1/amd$, $a = 0.37852$ nm, $c = 0.95139$ nm) are the two most stable polymorphs of TiO_2. Rutile is the only thermodynamically stable form of TiO_2, while anatase should be regarded as a metastable form, which can be formed in bulk at low temperature due to either kinetic or size effects. $\Delta G°$ of TiO_2(anatase) to TiO_2(rutile) transformation is about -5 kJ/mol at 298 K and this value does not vary significantly with temperature.[47,48] Once formed, anatase transforms irreversibly to rutile on heating above 600 °C.[47,49]

Epitaxial films of both TiO_2 polymorphs have been grown by a number of techniques with a thickness of up to 1 μm. Chen et al.[50] have succeeded in growth of epitaxial anatase thin films on (001)$SrTiO_3$ substrates by ultrahigh vacuum metal−organic chemical vapor deposition (MOCVD). The films have been comprehensively characterized by RHEED, XRD, HRTEM, and AES. The epitaxial relations reported were as follows:

$$(001)\,[100]_{\text{anatase}} \,||\, (001)\,[100]_{SrTiO_3}$$

These relations are due to low lattice mismatch between anatase and $SrTiO_3$ structures in the (001) plane, -3.1%. Pure anatase was formed on $SrTiO_3$ substrate in the whole temperature interval studied (250−800 °C). No transformation to rutile structure has been observed after annealing at 900 °C in air for 1 h. The epitaxial growth of anatase has also been achieved by other authors on lattice-matched (001)$SrTiO_3$,[51,52] (001)-$LaAlO_3$,[53,54] (001)$La_{0.5}Sr_{0.5}CoO_3$,[55] (001)MgO,[51] and (110)-MgO[51] substrates at 450−800 °C.

The phase mixture of oriented anatase and rutile was observed on (0001)Al_2O_3 substrates under the same deposition conditions;[50,51,56] the content of rutile increased with the growth temperature. The epitaxial relations reported are

$$(112)\,[1\bar{1}0]_{\text{anatase}} \,||\, (0001)\,[\bar{1}100]_{Al_2O_3}$$

$$(100)\,[001]_{\text{anatase}} \,||\, (0001)\,[10\bar{1}0]_{Al_2O_3}$$

In this case, both polymorphs have close lattice matches to the substrate and epitaxial stabilization of pure anatase is possible only at low temperature.

Phase pure epitaxial rutile films can be easily grown on $(1\bar{1}02)Al_2O_3$ in a wide temperature interval, 250−800 °C.[50,57] The epitaxial relations in this case are

$$(101)\,[010]_{\text{rutile}} \,||\, (1\bar{1}02)\,[\bar{1}\bar{1}20]_{Al_2O_3}$$

The epitaxial growth was due to a relatively small lattice mismatch between rutile and Al_2O_3 at the interface formed (-3.6% along the $[010]_{\text{rutile}}$ direction and $+6.4\%$ along the $[101]_{\text{rutile}}$ direction). Logically, no formation of epitaxial anatase on $(1\bar{1}02)Al_2O_3$ has been observed.

We undertook MOCVD of 200-nm-thick TiO_2 films at 800 and 1000 °C simultaneously on $(1\bar{1}02)Al_2O_3$ and perovskites ($LaAlO_3$, $SrTiO_3$).[58] In accordance with previous reports, we have observed the formation of phase pure rutile on sapphire and anatase on perovskites. The epitaxial relations found were just as described above. The measured lattice parameters of rutile and anatase coincided with those of the bulk materials within an experimental error. This fact confirms the absence of significant lattice strain in our films. Simultaneous growth of two different polymorphs on two different substrates at a temperature as high as 1000 °C is clear evidence for the thermodynamic epitaxial stabilization of anatase.

The epitaxial stabilization of anatase can be of practical importance. As compared to rutile, anatase films have been found to be more effective for photocatalytic[52,54] and photovoltaic[55] applications.

B. ZnO. Zinc oxide is a promising transparent conductor and luminescent material. It has been profoundly studied in past years. Epitaxial films of the stable in bulk hexagonal wurtzite form of ZnO (space group $P6_3mc$, $a = 0.32498$ nm, $c = 0.52066$ nm) can be readily obtained by various deposition techniques on single-crystalline Al_2O_3, $MgAl_2O_4$, GaAs, and InP substrates.[59−63]

Recently, pure ZnO epitaxial films with an unstable in bulk cubic zinc blend structure have been grown on (001)GaAs substrates with a cubic (001)ZnS buffer layer.[64] The growth has been performed with the use of metal−organic MBE at 550−600 °C. The ZnO film was shown to grow pseudomorphically with a ZnS substrate up to at least 560-nm film thickness. High epitaxial quality of ZnO layers has been proven with the use of RHEED, XRD, and HRTEM. The films have been found to be strongly tetragonally distorted (in-plane lattice parameter of 0.458 nm and out-of-plane lattice parameter of 0.436 nm). The pseudocubic lattice constant of the zinc-blend ZnO was 0.4505 nm, very close to the theoretically calculated value of 0.460 nm.[65] Evidently, this distortion appears as a consequence of large lattice

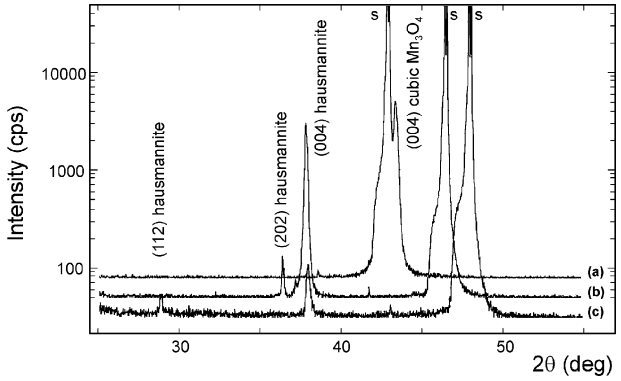

Figure 1. XRD patterns of Mn_3O_4 films grown on different substrates ($\theta-2\theta$ scans). (a) (001)MgO; (b) (001)$SrTiO_3$; (c) (001)$LaAlO_3$. Indices "s" denote substrate reflections.

mismatch with ZnS ($a = 0.5406$ nm). Nevertheless, the lattice mismatch for the strained layer remains quite large (−15%), leading to the high dislocation density on the film/substrate interface.

This result is of peculiar interest because it demonstrates the possibility of epitaxial stabilization even in the case of a large lattice mismatch when only partial strain relaxation occurs.

C. Mn_3O_4. Mn_3O_4 is an oxide with a spinel structure. The stable room temperature form is tetragonal hausmannite (space group $I4_1/amd$, $a = 0.5762$ nm, $c = 0.9470$ nm) with Mn^{3+} in the octahedral positions and Mn^{2+} in the tetrahedral positions of the spinel lattice. The oxygen octahedra are tetragonally distorted due to the Jahn−Teller effect on Mn^{3+} ions. The Jahn−Teller transition (JTT) in Mn_3O_4 occurs at 1160 °C.[66] The high-temperature form of Mn_3O_4 is cubic (space group $Fd3m$, $a = 0.842$ nm). Depending on the substrate temperature, both polymorphs can be grown as epitaxial films on MgO in the stability range of hausmannite.

Recently, the epitaxy of the hausmannite with (001) orientation on MgO by MBE was observed.[67,68] The deposition temperature in this study was much lower than the JTT temperature. In our work the growth of Mn_3O_4 films on MgO was performed by MOCVD at higher temperature.[69] Thin films of 100-nm thickness were grown at 750 °C in the oxygen−argon flow (total pressure 6 mbar, oxygen partial pressure 1 mbar) on single-crystal (001)$SrTiO_3$, (001)MgO, and (001)$LaAlO_3$ substrates. Simultaneous deposition allows neglect of process-related variations of the oxygen stoichiometry from one deposition run to another. Films on the perovskite substrates contained multiple-orientated hausmannite. The film on MgO according to XRD was found to be nearly cubic with the lattice parameter close to that of the Mn_3O_4 high-temperature form (Figure 1). The FWHM value of the rocking curve for the (004) peak of Mn_3O_4 was about 0.2°. HRTEM revealed weak tetragonal distortion in this film due to the epitaxial strain.[69] The film−substrate interface was fully coherent (Figure 2).

The high-temperature cubic form of Mn_3O_4 possesses essentially lower lattice mismatch with MgO than hausmannite (less than 0.1% instead of −3.3% for the *c*-domains of hausmannite). Respectively, a strained thin film of the cubic Mn_3O_4 becomes commensurable with the substrate and tetragonal, while hausmannite rather would form an incommensurate interface. Thus,

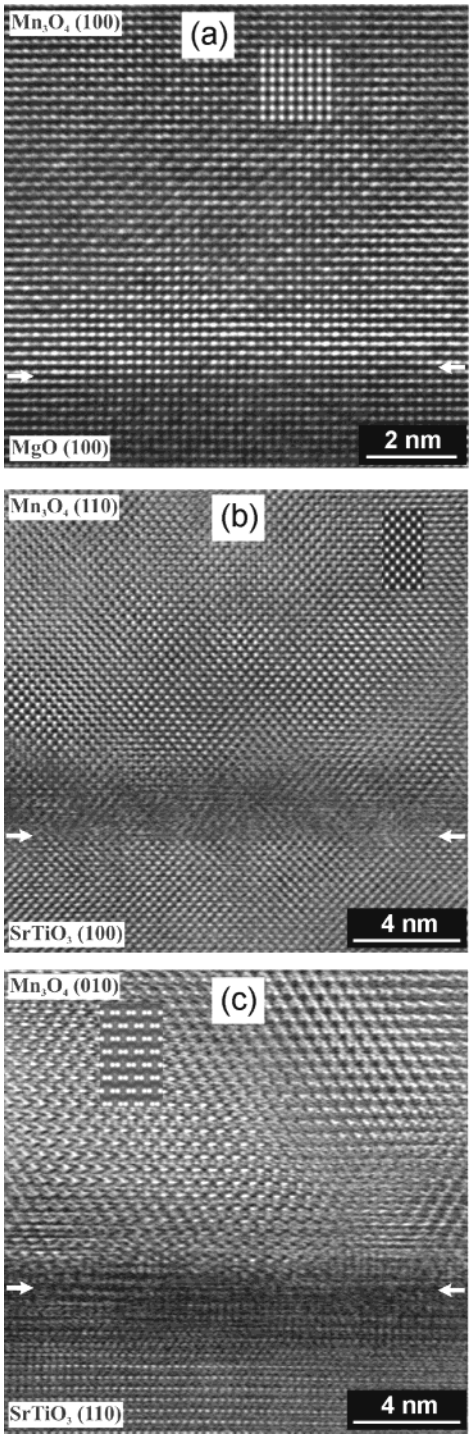

Figure 2. (a) HRTEM image of the cross section of a Mn_3O_4/MgO film. Inset shows simulated image based on the structure of the high-temperature form of Mn_3O_4. (b,c) HRTEM images of the Mn_3O_4 film on $SrTiO_3$. Insets show simulated images based on the hausmannite structure.

the gain of the interface energy compensates the Jahn−Teller distortion energy and it induces the decrease of JTT temperature from 1160 °C to below 750 °C.

D. WO_3. Tungsten trioxide undergoes several phase transitions under heating. The lattice symmetry consequently changes from triclinic (below 17 °C) through monoclinic (17−320 °C) and orthorhombic (320−720 °C) to tetragonal (above 720 °C).[70−72] LeGore et al. succeeded in the growth of (001)-epitaxial films of tetragonal WO_3 on $(1\bar{1}02)Al_2O_3$ substrates at 600 °C with the

use of electron-beam evaporation.[73] The phase composition was deduced from RHEED measurements. The films of pure tetragonal WO_3 could be grown only up to 30-nm thickness; the admixture of monoclinic and/or orthorhombic forms appeared in thicker films. The lattice mismatch for the tetragonal phase and $(1\bar{1}02)$ sapphire plane is +10.3% and +2.5% in the two perpendicular directions, while it is about +5% and +8% for both monoclinic and orthorhombic forms of WO_3.

E. Fe_2O_3. Maghemite, γ-Fe2O3, with a cubic spinel-related structure (a = 0.83515 nm) is a metastable polymorph, which irreversibly transforms to a hexagonal α-Fe_2O_3 form (hematite, space group $R\bar{3}c$, a = 0.50356 nm, c = 1.37489 nm) when heated.

It was possible to grow 100-nm-thick high-quality γ-Fe_2O_3 epitaxial films by MBE in the temperature range between 250 and 500 °C.[74] The films have been characterized with the use of RHEED, LEED, and XPS. γ-Fe_2O_3 was grown on (001)MgO substrate possessing a good lattice match of −0.9% with the γ-Fe_2O_3 structure. The epitaxial relations were as follows:

$$(001)\,[100]_{\gamma\text{-}Fe_2O_3} \,||\, (001)\,[100]_{MgO}$$

On the other hand, 30-nm-thick epitaxial films of the stable α-Fe_2O_3 in (0001), $(11\bar{2}0)$, and $(1\bar{1}02)$ orientations have been grown under exactly the same deposition conditions on sapphire of corresponding cuts.[75] α-Fe_2O_3 possesses the same corundum structure as sapphire and the lattice mismatch between these two structures in various orientations is about 5.6%. The epitaxial quality and phase composition of these films have been controlled with RHEED, LEED, XPS, and XRD.

IIb. Solid Solutions and Complex Oxides. *A. $Zn_{1-x}M_xO$ (M = Mg, Mn).* Zinc in wurtzite ZnO can be substituted to some extent by divalent cations with similar ionic radius, such as Mg^{2+}, Cd^{2+}, or Mn^{2+}. The MO solubility in bulk wurtzite $Zn_{1-x}M_xO$ does not exceed 0.02−0.04 for M = Mg and ≈0.13 for M = Mn according to refs 76 and 77, respectively.

However, single-phase (0001)$Zn_{1-x}Mg_xO$ epitaxial films with $x \le 0.22$ have been successfully grown by laser MBE at 550 °C[78−80] and with $x \le 0.36$ by PLD at 700−750 °C.[81] In both cases two-phase ceramic pellets have been used as targets, (0001)Al_2O_3 was used as a substrate, and the film thickness was 150 nm[78−80] and ≤500 nm.[81] High-crystalline quality of these films has been proved by XRD,[80,81] RBS channeling, and HRTEM.[81] The epitaxial relations found in ref 81

$$(0001)\,[\bar{1}2\bar{1}0]_{ZnMgO} \,||\, (0001)\,[01\bar{1}0]_{Al_2O_3}$$

are the same as those of wurtzite ZnO films grown on sapphire.[59] This corresponds to a lattice mismatch of 15%, which is the cause for the high dislocation density observed.[81] Additionally, it has been shown that $Zn_{0.85}Mg_{0.15}O$ layers are stable upon 1-h annealing at 1000 °C at 1 bar of oxygen, while the same heat treatment of $Zn_{0.78}Mg_{0.22}O$ film led to the decomposition, resulting in a stable phase mixture of wurtzite $Zn_{0.85}Mg_{0.15}O$ and rock-salt $Mg_{0.46}Zn_{0.54}O$ solid solutions.[80] Thus, there is a remarkable change in the T−x phase diagram of a MgO−ZnO binary system caused by the epitaxial stabilization effect.

Analogously, (0001)$Zn_{1-x}Mn_xO$/(0001)Al_2O_3 epitaxial films have been reported by Fukumura et al.[82] Several hundred nanometer thick layers have been grown by PLD at 600 °C and characterized by XRD. The wurtzite structure with a monotonic increase of a and c lattice parameters has been observed up to x = 0.35, well beyond the equilibrium solubility limit for a bulk state (x_{lim} = 0.13).[77]

B. $BaRuO_3$. At normal pressure, the stable in bulk form of barium ruthenate is a nine-layer rhombohedral phase (9R, a = 0.575 nm, c = 2.16 nm). Two other hexagonal phases have also been described: (4H, a = 0.573 nm, c = 0.95 nm; 6H, a = 0.571 nm, c = 1.410 nm).[83−86] For high pressures above 12 GPa a cubic-like perovskite polymorph of $BaRuO_3$ was predicted.[86] The cubic lattice constant of $BaRuO_3$ perovskite estimated from extrapolated data for $Sr_{1-x}Ba_xRuO_3$ solid solution is about 0.401 nm.[86]

Lee et al. have successfully grown and comprehensively characterized epitaxial films of 4H- and 9R-$BaRuO_3$ on (111)$SrTiO_3$ [87] and (001)$SrTiO_3$.[88,89] A number of other oxide substrates have been tried, but only the polycrystalline films with 4H structure could be grown on them. On (001)$SrTiO_3$ substrates a 4H-$BaRuO_3$ polymorph was found to grow with $(02\bar{2}3)$ orientation, while 9R-$BaRuO_3$ was with $(20\bar{2}5)$ orientation. The growth has been performed between 550 and 750 °C and the film thickness was between 90 and 460 nm. Ninety degree off-axis sputtering and PLD have been employed. The $BaRuO_3$ structure has been found to depend not only on substrate orientation but also on the growth temperature and growth technique used.[89] The lattice mismatch between these two polymorphs of $BaRuO_3$ and $SrTiO_3$ is about 4−5% for various crystal planes.

Fukushima et al.[90,91] reported on the growth of highly tetragonally distorted (c = 0.425 nm) $BaRuO_3$ epitaxial films with a perovskite structure on (001)$SrTiO_3$ using radio frequency (rf) sputtering. The film thickness was 50−100 nm, while the growth temperature has not been reported. This controversive result caused a comment by Lettieri et al.,[92] supposing that the films grown were indeed 9R-$BaRuO_3$. In their response Fukushima et al.[93] provided XRD reciprocal lattice maps and electron diffraction of their films, proving the tetragonal perovskite structure of $BaRuO_3$.

The discrepancies mentioned can be understood taking into account the structural, dimensional, and energetic similarity of different $BaRuO_3$ polymorphs. Thus, tiny variations in the growth conditions can cause the stabilization of a particular structure of $BaRuO_3$.

The report of Christen et al.[94] is of some interest in this connection. They failed to grow with a laser ablation $BaRuO_3$ perovskite on cubic (001)$KTaO_3$ (a = 0.3989 nm) substrate, even though it is well-matched to the predicted perovskite structure of $BaRuO_3$.[86] However, the PLD growth of 600-nm-thick epitaxial films of cubic $Sr(Ru_{0.5}Sn_{0.5})O_3$ solid solution, which was also claimed to be unstable in bulk, has been achieved at 750 °C. The cubic lattice constant of $Sr(Ru_{0.5}Sn_{0.5})O_3$ is about 0.399 nm, providing a very good match with $KTaO_3$. Partial substitution of Ba for Sr in $BaRuO_3$ makes stabilization of the perovskite phase in film easier as well.[91] Both substitutions (Sr for Ba and Sn for Ru) lead to the

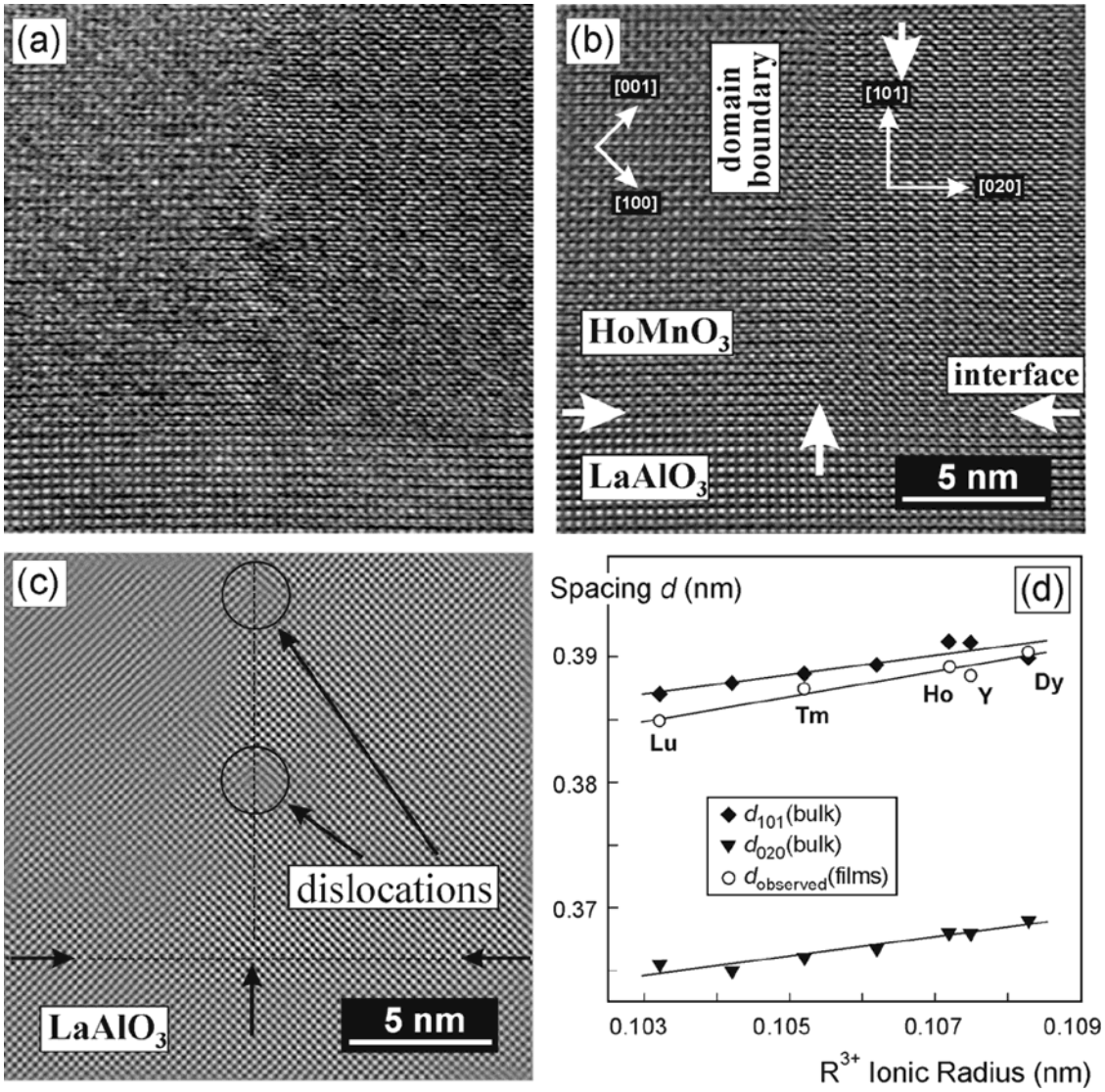

Figure 3. HRTEM and XRD characterization of $RMnO_3$ perovskite films: (a) HRTEM image of the film cross section including orthorhombic domain boundary; (b) the filtered image demonstrating the orientation of the doubling *b* axis along the film−substrate interface; (c) dislocations at the low-angle boundary formed by orthorhombic domains; (d) XRD data revealing (101) orientation of $RMnO_3$ films on (001)$LaAlO_3$.

decrease of the Goldshmidt tolerance factor of $BaRuO_3$ ($t = 1.00$), resulting in the increase of the compound stability.

C. $BaTi_{1-x}Nb_xO_3$. Barium titanate doped with niobium is a perspective material due to its ferroelectric properties. $BaTi_{1-x}Nb_xO_3$ ($x = 0.01$, 0.02, 0.03, 0.10, and 0.15) epitaxial films have been grown by laser ablation with hexagonal and stable in bulk perovskite structures.[95] The depositions have been performed at 700 °C on the (0001)Al_2O_3 substrate and at 650 °C on a (001)-$SrTiO_3$ substrate, respectively. The resulting lattice mismatches with corresponding polymorphous forms of $BaTi_{1-x}Nb_xO_3$ are 17% for the Al_2O_3 substrate and 3.2% for the $SrTiO_3$ substrate, if the data for the bulk forms of $BaTi_{1-x}Nb_xO_3$ are taken into account. However, the *c* lattice constant measured deviated significantly from that of the bulk form. Possible reasons could be the oxygen deficiency, inaccuracy of Ti/Nb ratio determination, or strain in films. The latter is rather possible because of the small film thickness (60 nm) and relatively low growth temperature used. The satisfactory epitaxial quality of layers is evidenced by low FWHM's of rocking curves (0.91° for the hexagonal form and 0.58° for perovskite).

D. $RMnO_3$. In the sequence of $RMnO_3$ compounds the perovskite phase does not exist under ambient pressure for the rare earth elements with small ionic radius (Y, Ho−Lu). The normal pressure phase has a hexagonal structure.[96] A corresponding $RMnO_3$ perovskite structure was obtained only under high pressure.[97] Nevertheless, the surface contribution to free energy can change the situation—$YMnO_3$ nanoparticles have been reported to adopt the perovskite structure instead of the hexagonal one.[98]

The epitaxial stabilization of $RMnO_3$ phases (R = Ho, Y, Tm, Lu) in the perovskite form was demonstrated by MOCVD on (001)$LaAlO_3$ and (001)$SrTiO_3$.[99] The most effective stabilization took place on the $LaAlO_3$ substrate due to the lowest lattice mismatch (0.5%). The films with the thickness of 100−200 nm were deposited at 750 °C. Under the same conditions no perovskite phase was found on $(1\bar{1}02)Al_2O_3$ and (111)$ZrO_2(Y_2O_3)$ substrates. Orthorhombic $YMnO_3$ was also grown by PLD.[100]

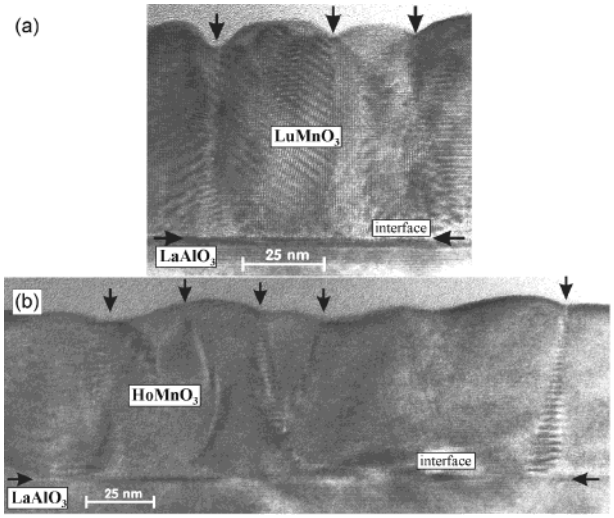

Figure 4. TEM images of cross sections of $RMnO_3$ perovskite films. (a) $LuMnO_3/LaAlO_3$; (b) $HoMnO_3/LaAlO_3$. Black arrows indicate domain boundaries and the film−substrate interface.

In accordance with the data for high-pressure bulk $RMnO_3$, the perovskite films prepared possessed a high orthorhombic distortion (about 5%, space group *Pnma*). This distortion is responsible for the orthorhombic twinning in the film. The twinning was observed to be selective in the films on $LaAlO_3$—the doubling axis was found by XRD and HRTEM always in the film plane. Indeed, as can be seen from the HREM image (Figure 3b) and the lattice spacing of observed XRD reflections (Figure 3(d)), $RMnO_3$ films grew with (101) orientation without any admixture of (010)-oriented grains. This twinning type minimizes the film−substrate lattice mismatch. Domains form a regular sequence by 90° switching of the doubling axis orientation in the neighboring domains. The domain size correlates with the mismatch at the interface between the film and the substrate (Figure 4). Thus, essentially larger domains were observed for $HoMnO_3$ (mean grain size of 60 nm), as compared to those of $LuMnO_3$ (30 nm).

$RMnO_3$ perovskites are a good example for demonstrating that the lattice strain is actually not necessary for the epitaxial stabilization to occur. Being an orthorhombic perovskite, the film adopts the periodic multiple-domain structure formed by orthorhombic twins, providing the essential reduction of the interface energy in accordance with the theory by Little and Zangwill.[31]

E. β-BaB_2O_4. This compound is one of the most important nonlinear crystals in laser optics. Fabrication of hexagonal β-BaB_2O_4 (space group $R\bar{3}c$, $a = 1.253$ nm, $c = 1.273$ nm) thin films is difficult because of the complex crystal structure and a polymorphic transition at around 925 °C to a high-temperature solid phase, α-BaB_2O_4, which has no optical nonlinearity. In polycrystalline thin films the polymorphic transition occurs even at lower temperature. For instance, the transition was observed already at 650 °C in BaB_2O_4 polycrystalline random films on (001)Si. However, single-phase (001)-oriented β-BaB_2O_4 films could be grown by magnetron sputtering,[101] PLD,[102] and MOCVD[103] on (0001) and $(1\bar{1}02)$ sapphire substrates without any admixture of α-BaB_2O_4 under the same process conditions up to 750 °C. The film thickness was up to 500 nm.

III. Epitaxial Stabilization of Unusual Stoichiometric Types

Epitaxial stabilization can be the cause of the formation of complex oxides with unusual stoichiometry, which are absent on bulk $P-T-x$ phase diagrams under the growth conditions used. Four well-studied examples of such behavior are given in this section.

A. $BaCu_3O_4$. An important for synthesis of high-temperature superconductors Ba−Cu−O system has been intensively investigated. Thermodynamic stability under various $p(O_2)-T$ conditions has been proven so far only for Ba_2CuO_{3+x}, $BaCuO_{2+y}$, $Ba_2Cu_3O_{5+z}$, and $BaCu_2O_{2+w}$, while $BaCu_3O_4$ is believed to be a metastable phase.[104,105]

$BaCu_3O_4$ was first reported by Bertinotti et al. as an oriented impurity phase appearing in $YBa_2Cu_3O_{7-\delta}$ single crystals.[106] The unit cell of $BaCu_3O_4$ is an orthorhombic one with a *Cmmm* space group and unit cell parameters of $a = 1.101(2)$ nm, $b = 0.550(1)$ nm, and $c = 0.3923(2)$ nm. The structure consists of alternating Cu_3O_4 and Ba layers along the *c* axis and is closely related to that of infinite layer and spin ladder compounds.[107,108] $BaCu_3O_4$ can be considered as a member of the $A_{n-1}Cu_{n+1}O_{2n}$ structural family with A = Ba and $n = 2$.

The epitaxial stabilization and study of $BaCu_3O_4$ thin films on perovskite single-crystalline substrates as well as a secondary phase in epitaxial (001)$RBa_2Cu_3O_7$ films have been reported by us in refs 109−113. The epitaxial relations with ABO_3 perovskite substrates ($LaAlO_3$ or $SrTiO_3$) were found to be as follows,

$$(001)\,[210]_{BaCu_3O_4} \,||\, (001)\,[100]_{ABO_3} \text{ and } (001)\,[210]_{BaCu_3O_4} \,||\, (001)\,[010]_{ABO_3}$$

$$(210)\,[001]_{BaCu_3O_4} \,||\, (001)\,[100]_{ABO_3} \text{ and } (210)\,[001]_{BaCu_3O_4} \,||\, (001)\,[010]_{ABO_3}$$

which corresponds to the lattice mismatch of <2%. The crystal structure and lattice parameters of $BaCu_3O_4$ were determined with the use of electron diffraction and XRD.[111] No difference was found for $BaCu_3O_4$ grown on different substrates and the parameters found coincided with those observed by Bertinotti et al.[106] Thus, $BaCu_3O_4$ films were not strained.

It is known that the decrease of the interface energy can be realized by the formation of a multiple-domain structure, as it takes place in some orthorhombic perovskites (Figure 3). However, $BaCu_3O_4$ films consisted of separate islands (Figure 5). Noteworthy, this possibility has not yet been accounted for in epitaxial stabilization theory. The growth mode observed is probably because of the $BaCu_3O_4$ structure anisotropy that does not permit the formation of low-energy domain walls.

It was also found that $BaCu_3O_4$ phase is stable in films only until some critical thickness (the average value was taken into account because of the films' island structure); for (001)$BaCu_3O_4$ films grown on (001)-$LaAlO_3$ the critical value was found to be 300 nm. The decomposition of $BaCu_3O_4$ in thicker films took place according to the reaction

$$BaCu_3O_4 \rightarrow BaCuO_2 + 2CuO$$

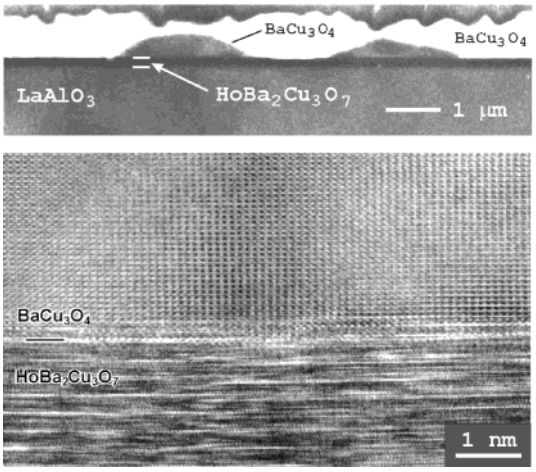

Figure 5. TEM images of the cross section of a (001)-$HoBa_2Cu_3O_7/LaAlO_3$ film containing oriented $BaCu_3O_4$ secondary phase, which forms islands on the $HoBa_2Cu_3O_7$ film surface.

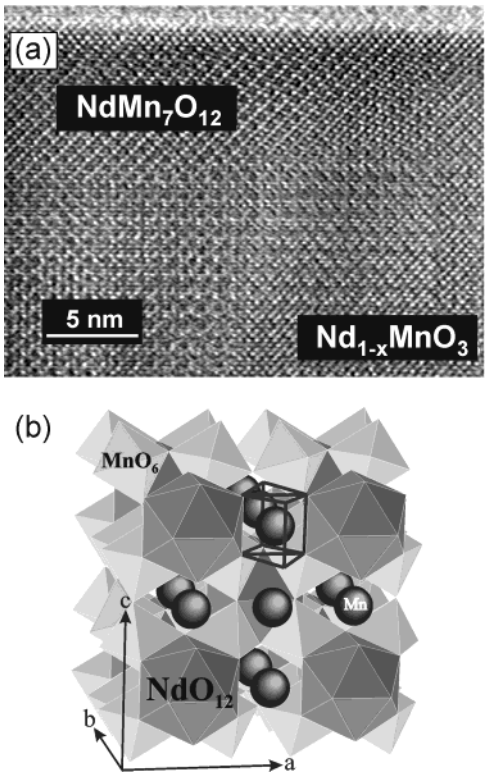

Figure 6. (a) HRTEM image of the $NdMn_7O_{12}/NdMnO_3$ epitaxial interface for the perovskite pseudocubic zone [100]. (b) Model of the crystal structure of the high-pressure $NdMn_7O_{12}$ phase.

Indeed, $BaCuO_2$ and CuO are the thermodynamically stable compounds of the Ba−Cu−O system in a bulk polycrystalline form for the deposition conditions used (T = 820 °C, $p(O_2)$ = 2 mbar).

B. $NdMn_7O_{12}$. In contrast to the bulk samples in Nd−Mn−O systems, thin films enriched with manganese up to a Nd:Mn ratio of ≈0.5 did not contain hausmannite Mn_3O_4 on the perovskite substrates, but another phase. This phase was observed as a 10-nm-thick island layer on a surface of 120-nm-thick perovskite film (Figure 6).[114] Electron diffraction, XRD patterns, and EDX analysis of this phase permit identification of it as $NdMn_7O_{12}$. The phase had strict epitaxial relations with the underlying perovskite manganite,

$$(001)\,[100]_{NdMn_7O_{12}} \,||\, (001)\,[100]_{Nd_{(1-x)}MnO_3}$$

(in a pseudocubic notation). Earlier, bulk $NdMn_7O_{12}$ phase was synthesized only under high pressure of 8 GPa at 1000 °C.[115] It is a perovskite-related compound with A-sites occupied by Nd and 3/7 Mn atoms (with the strongly distorted oxygen surrounding), while the remaining 4/7 Mn atoms occupy B-sites.

Noteworthy is that among high-pressure $RMnO_3$ perovskites (R = Ho−Lu,Y, see section IIb.D) and $NdMn_7O_{12}$ the latter needs essentially higher pressure for synthesis in bulk and, respectively, $NdMn_7O_{12}$ films can be grown only to significantly lower thickness as compared to $RMnO_3$.

C. $Bi_3Fe_5O_{12}$. $Bi_3Fe_5O_{12}$ with a garnet structure (cubic lattice constant a = 1.263 nm) is thermodynamically unstable due to the large size of Bi^{3+} cation. The ceramics sintered at 800−900 °C consisted of the phase mixture of $BiFeO_3$ and $Bi_2Fe_4O_9$.[114] It was however possible to stabilize the compound as an epitaxial film using a single-crystal garnet substrate, $Gd_3(ScGa)_5O_{12}$ (a = 1.263 nm, the lattice mismatch with $Bi_3Fe_5O_{12}$ of <0.5%). The epitaxial $Bi_3Fe_5O_{12}$ films in (001) and (111) orientations have been grown up to 1-μm thickness by reactive ion beam sintering,[116,117] electron cyclotron resonance,[118,119] rf sputtering,[118,119] and PLD[116,120,121] at temperatures around 550 °C. High epitaxial quality of the submicrometer layers was observed by XRD (FWHM of a (004) rocking curve was about 0.05°).[116]

D. Ba_2RuO_4. Ba_2RuO_4 with a K_2NiF_4 structure (a = 0.399 nm, c = 1.343 nm) can be synthesized in a polycrystalline form only using high pressure of at least 64 GPa.[122] Jia et al.[123] succeeded in the epitaxial growth of 150-nm-thick films of this compound at 1000 °C using PLD on (001)$SrTiO_3$ substrates (the lattice mismatch was 2.1%). The importance of the use of the well-matched substrates with a perovskite structure was especially stressed. No formation of Ba_2RuO_4 with a K_2NiF_4 structure has been observed under the same conditions on (001)MgO, (001)$MgAl_2O_4$, and (001)-$LaSrGaO_4$ and poor-matched perovskite (001)$LaAlO_3$ and (001)$LaAlO_3$−$Sr_2AlTiaO_6$ substrates.

IV. Change of the Phase Relations due to Epitaxial Stabilization

The change of phase relations due to epitaxial stabilization implies not only the appearance of new phases and phase fields but also the change of the phase fields of the compounds stable in bulk. This expands the importance of the epitaxial stabilization in thin film growth greatly. Here, we consider in detail the case of R−Ba−Cu−O films.

The $BaCuO_2$ phase can coexist in equilibrium with $YBa_2Cu_3O_7$ in polycrystalline samples.[104,105] However, the phase was not observed in our slightly off-stoichiometric (001)$RBa_2Cu_3O_7$ (R = Lu, Ho, Y, Gd, Nd) epitaxial films grown by MOCVD; instead, (001)-oriented Ba_2CuO_3 and $BaCu_3O_4$ were formed.[109]

Also, no formation of thermodynamically stable rare-earth-rich R_2BaCuO_5 secondary phases has been observed. Instead of R_2BaCuO_5 inclusions, platelike oriented R_2O_3 nanoinclusions of the 3−20-nm size were

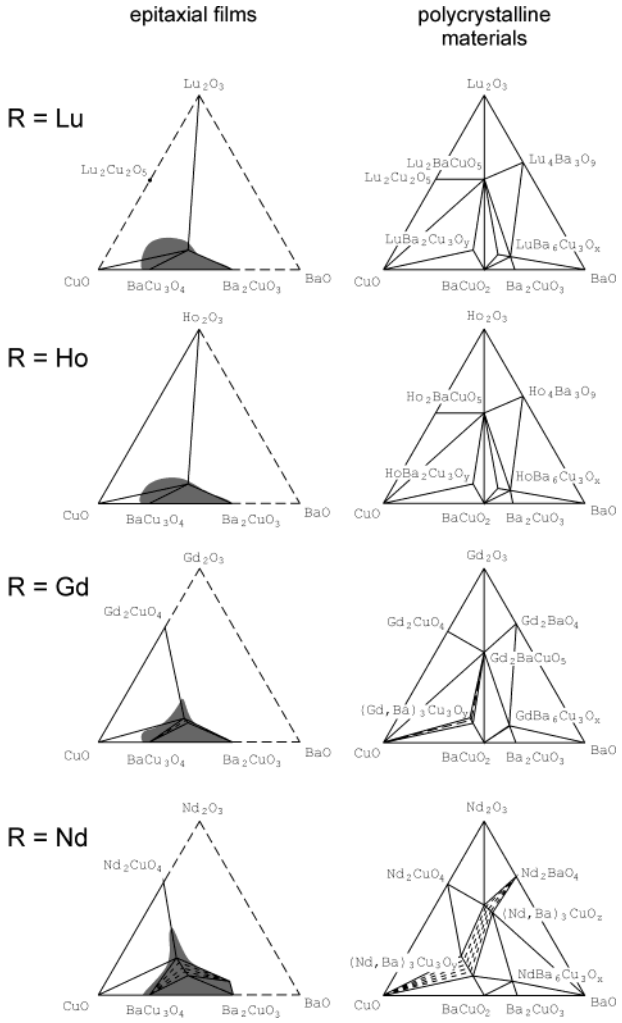

Figure 7. Phase relations in off-stoichiometric (001)-$RBa_2Cu_3O_7$ epitaxial films in comparison to the equilibrium phase diagrams of corresponding R−Ba−Cu−O systems in bulk (820 °C, $p(O_2) = 2$ mbar). These phase assemblies have been observed in films only for the cation compositions inside of the areas marked with gray color.

detected by HRTEM inside the film matrix if the films were slightly enriched with R. The epitaxial relations were as follows:

$$(001)\,[110]_{R_2O_3} \,||\, (001)\,[100]_{RBa_2Cu_3O_7}$$

These data are in good agreement with the observations reported by other authors for yttrium-enriched (001)-$YBa_2Cu_3O_7$ epitaxial films grown by various deposition techniques.[124−127] In contrast to the Lu, Ho, and Y systems, increasing Gd or Nd content in films resulted in the crystallization of (001)-oriented R_2CuO_4 phases together with $R_{1+x}Ba_{2-x}Cu_3O_7$ solid solutions.[112] Just like Ba_2CuO_3 and $BaCu_3O_4$, R_2O_3 and R_2CuO_4 phases have a good lattice match to the $RBa_2Cu_3O_7$ structure and the phase relations observed are not typical for the bulk-phase diagrams known for polycrystalline samples.[102,103] Secondary phase observations in epitaxial $RBa_2Cu_3O_7$ films are summarized in Figure 7. It is noteworthy that all the secondary phases observed in our (001)$RBa_2Cu_3O_7$ films, except for CuO, are believed to exist in nonequilibrium with bulk $RBa_2Cu_3O_7$. Nevertheless, being well-oriented, all these phases appear together with an epitaxial $RBa_2Cu_3O_7$ matrix, forming coherent or semicoherent grain boundaries with it.

Due to epitaxy, the nature of precipitating secondary phases is distinctly influenced by the substrate orientation. It has been shown that Y_2O_3 inclusions appear in yttrium-rich $YBa_2Cu_3O_7$ films grown on (001)MgO substrates, while on (110)MgO substrates the typical inclusions were Y_2BaCuO_5 particles.[128] Another interesting observation was the appearance of a well-oriented $Y_2Cu_2O_5$ secondary phase in $RBa_2Cu_3O_{7-\delta}$ films grown on (110)$ZrO_2(Y_2O_3)$.[129] Evidently, the oriented $Y_2Cu_2O_5$ secondary phase appears only due to a good lattice match with a (110)$ZrO_2(Y_2O_3)$ substrate (5% along the [100] substrate direction and −4% along the [110] substrate direction).

V. Epitaxial Stabilization Accompanied by a Change in the Metal Oxidation State

In some cases epitaxial stabilization makes possible stabilization of various oxidation states of a metal, thus influencing the $p(O_2)-T$ stability range of the oxide materials. Some important examples of such behavior are given in this section.

Va. Simple Metal Oxides. *A. CrO_2.* CrO_2 with a tetragonal rutile structure (space group $P4_2/mnm$, $a =$ 0.4421 nm, $c = 0.2916$ nm), an important for applications half-metal ferromagnet, is metastable at ambient pressure and irreversibly decomposes, forming Cr_2O_3 when heated above 200 °C.[130] According to phase diagrams, CrO_2 is thermodynamically stable only at very high oxygen pressure.[131] However, it was possible to deposit 1-μm-thick epitaxial films of CrO_2 at 1 bar of oxygen by CVD at temperatures as high as 450 °C.[132−136] CrO_3 or Cr_8O_{21} volatile oxides are usually used as precursors. Ivanov et al.[132] have shown that growth is possible, even in an argon atmosphere, though the films' crystallinity was poorer. Well-matched single-crystalline substrates are essential for CrO_2 growth; for this purpose TiO_2 in various orientations and (0001)Al_2O_3 are well-suited. CrO_2 films on (0001)Al_2O_3 had a multiple-domain structure with the b axis of CrO_2 aligned along three equivalent [11$\bar{2}$0] directions of Al_2O_3.[134] TiO_2 provides the lattice mismatch with CrO_2 of 2−4% depending on orientation. Gupta with co-authors[136] have also observed that CrO_2 does not form at all, being deposited onto an amorphous SiO_2 layer that enabled surface-selective growth of CrO_2 films on a patterned SiO_2/TiO_2 layer.

It should be noted that CrO_2 films can also be grown in a polycrystalline state if an isomorphous polycrystalline template is applied. Thus, CrO_2 layers have been grown on polycrystalline rutile thin films[136,137] and on rutile particles.[138]

B. MnO. MnO has a NaCl-type structure ($a = 0.444$ nm) and can be prepared in the bulk state only under very low oxygen pressure. Nevertheless, epitaxial (111)-MnO films 20−500-nm thick were grown on (0001)Al_2O_3 and (111)MgO substrates by PLD.[139] The Mn_2O_3 target was used, while growth was performed at 700 °C and $p(O_2) = 10^{-4}$ mbar, that is, well inside the stability field of Mn_3O_4. Indeed, at this temperature bulk MnO can be formed only at $p(O_2)$ below 10^{-8} mbar. The authors of the work believe that their results are only due to

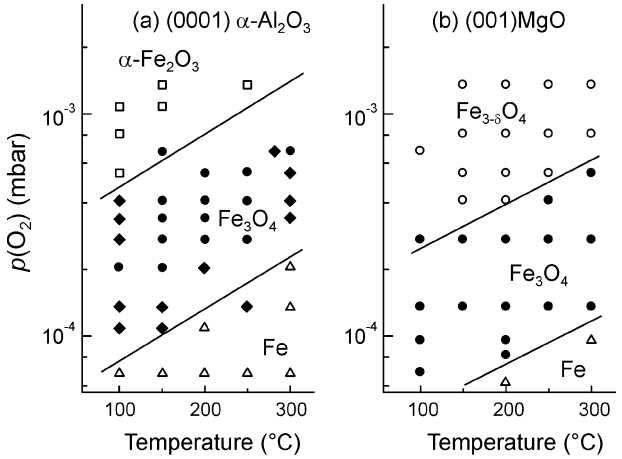

Figure 8. $p(O_2)-T$ deposition diagrams showing the phases observed in Fe−O films grown by MBE on sapphire and MgO substrates. The image is adopted from refs 140−142.

the nonequilibrium character of PLD. Taking into account that the oxidation of MnO is kinetically very easy even in UHV conditions,[140] we suppose that the origin of the MnO appearance is a thermodynamic one.

C. Fe−O System. This system is one of the most significant for practical purposes and possesses probably one of the most reliable phase diagrams available.[141] In this system a whole series of the epitaxial stabilization effects was observed, resulting in the drastic variation of the phase diagram as a function of the substrate material. A wealth of papers on that subject are available. The possible oxide phases in the Fe−O system are wustite ($Fe_{1-x}O$), magnetite (Fe_3O_4), maghemite (γ-Fe_2O_3), and hematite (α-Fe_2O_3). Maghemite is absent in the equilibrium Fe−O phase diagram. The phase has the same structure as magnetite and can be considered as the end member ($Fe_{2.67}O_4$) of the $Fe_{3-\delta}O_4$ solid solution. The consideration of maghemite as a separate phase makes sense, nevertheless, because of the great difference in electric and magnetic properties in relation to magnetite. At the same time, according to bulk equilibrium diagrams, the homogeneity limit of the spinel phase is close to that of stoichiometric Fe_3O_4. Wustite field appears on the equilibrium phase diagram only above 575 °C.

Most of the data on the epitaxy of iron oxides were obtained by O_2-plasma-assisted MBE. The first well-established fact is the crucial effect of the substrate on the phase composition of the iron oxide films. The effect can be easily seen from $p(O_2)-T$ diagrams reported (Figure 8).[142−144] On the MgO substrate, which possesses the lowest mismatch to magnetite, Fe_3O_4 can be obtained under the same conditions when one obtains hematite (at the high oxygen pressure) or metal iron (at the low oxygen pressure) on $(0001)Al_2O_3$. The transition from magnetite to hematite is discontinuous on $(0001)Al_2O_3$, which possesses the same corundum structure as a hematite with a lattice mismatch of 5.7%. In contrast, the full series of $Fe_{3-\delta}O_4$ solutions from magnetite to maghemite was grown on MgO under conditions when only hematite is stable on $(0001)Al_2O_3$.[74,75,142−150] The result seems to be understandable taking into account that the lattice mismatch of MgO with magnetite is 0.4% and that with maghemite is 0.8%.

One should note that in addition to the pronounced substrate effect the Fe−O system response to $p(O_2)-T$ variations follows thermodynamic regularities known for equilibrium diagrams, although plasma-assisted MBE is a highly nonequilibrium process by itself. Different iron oxides can be obtained in a systematic manner on the same substrate by variation of temperature and oxygen partial pressure. These results can be changed also by a too high deposition rate, resulting in the loss of epitaxy.

Another interesting phenomenon is stabilization of epitaxial wustite outside of its stability field in the bulk state. Two sets of data should be regarded here. First is the decrease of the temperature of the eutectoid decay of the $Fe_{1-x}O$ phase. In fact, no wustite field can be detected on the diagrams in Figure 8. But, as was shown by Gao et al.,[149] at a higher deposition temperature of 450 °C wustite films can be grown epitaxially on well-matched (001)MgO substrates (mismatch of 2.3%). Still, these conditions correspond to the coexistence of metallic Fe and Fe_3O_4 in bulk. Noteworthy, Gao et al.[149] believed that the stabilization of wustite was a kinetic one (but they consider at the same time the thermodynamic reasons for stabilization of maghemite) because of the very high sensitivity of the wustite formation to Fe/O ratio. We can suppose that this argument does not cancel out the thermodynamic reasons. In fact, wustite at eutectoid decomposition is a pointlike phase (the nonstoichiometry field becomes broad only at the higher temperature).

On the other hand, the competitive Fe_3O_4 phase has essentially lower mismatch with MgO than wustite. In that case, wustite could win thermodynamic competition with magnetite only for such a nearly singular Fe/O ratio, when it can grow as a *single-phase* epitaxial film instead of a Fe + Fe_3O_4 mixture. A two-phase assembly containing wustite should be energetically less favorable than the phase assembly containing a maximum amount of epitaxial magnetite on MgO: the latter provides a minimization of the free energy. There is probably no need to mention that the consideration works only in the case of the epitaxially stabilized wustite and is not applicable to the conditions when wustite is a phase, which is stable in bulk.

The second example of the wustite stabilization was observed at elevated temperatures (above 700 °C) and $p(O_2)$ corresponding to a magnetite stability field. It consists of the formation of epitaxial wustite films with a thickness not exceeding a few a monolayers on some metal substrates such as (111)Pt[151] and (001)Cu.[152] The common feature here is the conversion of these films to epitaxial $(111)Fe_3O_4$ with the increase of thickness.[153]

The third phenomenon to be discussed consists of the strong variation of the doping effects in iron oxides with the energy contribution of epitaxy. The stability field of a spinel-based Fe_3O_4 structure can be expanded significantly on the well-matched substrate. In particular, both Fe_3O_4 and NiO (rock salt structure) can grow epitaxially on MgO, but the former phase provides a better lattice match to the substrate. Respectively, in Fe_3O_4−NiO thin films the single-phase spinel is stable up to higher nickel content, as compared to the bulk state.[154] Moreover, it was found that a nickel−iron distribution between tetrahedral and octahedral posi-

tions of the epitaxial films (a degree of the spinel inversion) differs from that of the bulk material with the same Ni content.[154]

A better understanding of the epitaxial stabilization phenomena in the Fe−O system would have a significant impact on the practical application, taking into account the importance of the magnetite-based thin film materials for magnetic memories and sensors.

Vb. Complex Metal Oxides. *A. $RNiO_3$.* The whole series of perovskite rare earth nickelates $RNiO_3$ (except for R = La) can be prepared in bulk only under high oxygen pressure of 100 bar.[155] In contrast to $RMnO_3$, when external high pressure stabilizes the perovskite phase, an increase of the chemical potential of oxygen is necessary to obtain $RNiO_3$ as a bulk perovskite.

The preparation of thin epitaxial $RNiO_3$ films for R = Pr, Nd, Sm, Gd was accomplished by MOCVD.[156] It is peculiar that the preparation was successfully done at reduced oxygen partial pressure (<20 mbar). The epitaxy of $NdNiO_3$ by PLD has also been reported.[157] $RNiO_3$ phase is formed only in R−Ni−O films deposited on perovskite substrates ($LaAlO_3$, $SrTiO_3$), while the films on MgO and $ZrO_2(Y_2O_3)$ consisted of rare-earth oxide and NiO phase mixture. Single-phase $RNiO_3$ films were obtained only on $LaAlO_3$ substrates possessing the lowest lattice mismatch (0.2−0.7%). The $RNiO_3 + R_2O_3 + NiO$ phase mixture was found in the films grown on substrates with larger mismatch, for example, $SrTiO_3$ (≈3%). The difficulty in obtaining epitaxial perovskite $RNiO_3$ films increases with the decrease of R^{3+} ionic radius. This is the manifestation of the well-known decrease of thermodynamic stability of various rare-earth-containing perovskites in the same sequence.[158] The least stable nickelate studied, $GdNiO_3$, could be obtained only on a perfectly matched $LaAlO_3$ substrate. A clear correlation between free energy of the perovskite nickelate formation and the critical thickness of the layer was demonstrated.[156] At the thickness exceeding the critical value the growth of a simple oxides mixture ($R_2O_3 + NiO$) started.

The atomically flat coherent interfaces between $RNiO_3$ and $LaAlO_3$ have been observed by HRTEM. No misfit dislocations were observed, indicating that the tetragonal lattice strain must be present in the film; this conclusion has been confirmed by XRD study.[157]

The films were found to be orthorhombic (space group *Pnma*), consisting of domains including all three possible directions of the doubling axis (Figure 9). Noteworthy, the orthorhombic distortion in nickelate films was quite modest in comparison to that in $RMnO_3$ (see Section IIb.D) Thus, orthorhombic domains all have nearly the same mismatch with the substrate. In this case orthorhombic twinning cannot contribute significantly to strain relaxation and the perovskite film must keep the epitaxial lattice strain. It should be outlined that the anisotropic lattice strain is a destabilizing factor and, along with the lattice mismatch, it suppresses the growth of $RNiO_3$ perovskites, decreasing the critical thickness.

The cross-section HRTEM pictures show (Figure 10) that the perovskite nickelate and products of their decomposition coexist in the broad range of the film thickness. The area occupied by the perovskite phase gradually decreases with the film thickness. The structure of nickelate films with the thickness exceeding the critical value (like in the case of the $SrTiO_3$ substrate) is an excellent demonstration of the validity of an idea about gradual character of transition from the epitaxially stabilized phase to the stable in bulk products.[31] We have also succeeded in the growth of composites with a columnar structure. These films consisted of a $RNiO_3 + NiO$ phase mixture, although under the growth conditions bulk $RNiO_3$ decomposes to NiO and R_2O_3. The stable coexistence of epitaxially stabilized and stable in bulk phases confirms the thermodynamic origin of the stabilization effect; that is, $RNiO_3$ in thin epitaxial films must be regarded as a thermodynamically stable phase.

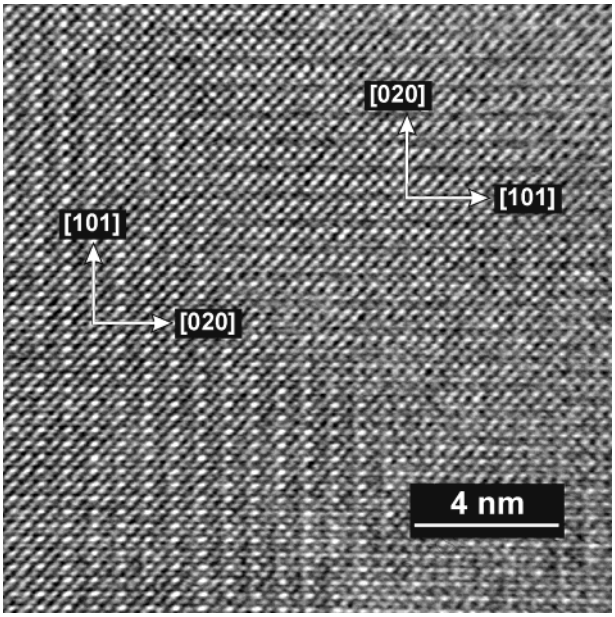

Figure 9. HRTEM of $NdNiO_3/LaAlO_3$ film cross sections: orthorhombic domains. The doubling of the *b* lattice parameter is observed both parallel and normal to the film−substrate interface (horizontal). Note that the result is in contrast to the behavior of $RMnO_3$ films on $LaAlO_3$ (Figure 4) where the doubling axis is always parallel to the film−substrate interface.

The epitaxial stabilization of nickelates allowed us to carry out selective MOCVD growth of $NdNiO_3$ on $(La,Pr)_{0.7}Ca_{0.3}MnO_3$ epitaxial film patterned by a polycrystalline CuO layer deposited over manganite film.[160,161] In this case the nickelate epitaxial layer was selectively formed only on a bare manganite surface due to a close lattice match of their structures. In contrast, no $NdNiO_3$ formation was observed in areas covered with CuO.

B. $LaCuO_{3-\delta}$. $LaCuO_{3-\delta}$ perovskite attracted much attention as a parent structure to the high-temperature superconducting cuprates. A stoichiometric ($\delta = 0$) rhombohedrally distorted phase can be prepared only under very high oxygen pressure, but it loses oxygen when heated above 150 °C.[162] A series of oxygen-deficient $LaCuO_{3-\delta}$ phases with different types of oxygen vacancies ordering was reported. In particular, the monoclinic phase with $0.2 < \delta < 0.5$ (space group *C*2/*c*) is stable in air under ambient pressure. The orthorhombic modification with $\delta = 0.5$ (space group *Pbam*, $a = 0.55482$ nm, $b = 1.04677$ nm, $c = 0.38801$ nm) has been prepared under a pressure of 6 GPa.[163]

PLD of 300-nm-thick $LaCuO_{3-\delta}$ films on (001)$SrTiO_3$ substrates at 650−750 °C and $p(O_2) = 0.26$ mbar

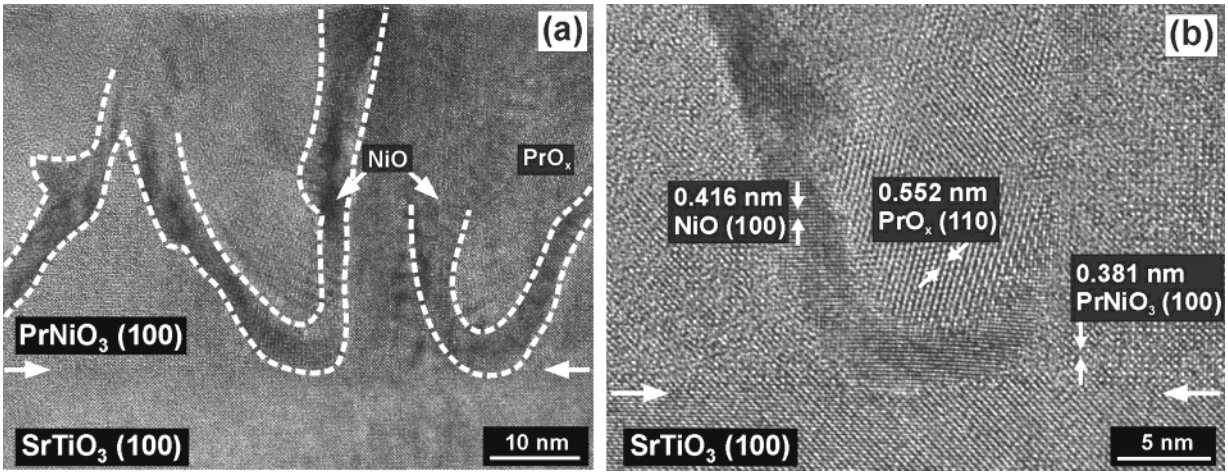

Figure 10. Pr−Ni−O film on $SrTiO_3$. HRTEM observations of the phase composition change through the film thickness. Phase pure $PrNiO_3$ perovskite is observed only near the film−substrate interface, while the decomposition to NiO and PrO_x occurs as the film thickness increases.

resulted in the epitaxial growth of the orthorhombic $LaCuO_{2.5}$ high-pressure phase with the (120) plane parallel to the substrate surface.[164] Postannealing of these films in oxygen allowed their conversion to the oxygen-enriched monoclinic phase with mixed ($2\bar{1}0$), (120), and (001) orientations. The films have been characterized by XRD, electron diffraction, and TEM. The out-of-plane lattice parameter of the pseudocubic cell for the orthorhombic phase was found to be 0.3845 nm. Taking into account the lattice parameters reported for the bulk material,[161] the mismatch between orthorhombic $LaCuO_{2.5}$ and $SrTiO_3$ is −2.3% and −0.6% along two perpendicular directions in the interface plane.

VI. Considerations of the Mechanism and Limits of Epitaxial Stabilization of Oxides

Thus, there are many experimental facts of the epitaxial stabilization in thin films, which cannot be explained by kinetic reasons of any kind or only by pressure effect developed in the strained film (Table 2). The epitaxial stabilization model of Zunger and Wood[34−36] is hardly applicable to oxide systems when semicoherent or noncoherent interfaces form very easily, even at small film thickness. The behavior of oxides in thin films has more conformity with the model of Little and Zangwill,[31] accounting for the interface incoherency. Nevertheless, the bulk free energy term in the model seems to be highly overestimated in this case and the actual field of the epitaxial stabilization is much broader than that in the standard phase diagrams of the model. In the following, thermodynamic considerations describing the epitaxial stabilization phenomenon are presented.

For the nucleus of the growing phase the following expression for the Gibbs' energy can be written,

$$\Delta G_f = \Delta g V + \sigma S + \Delta G^{\text{stress}} \quad (1)$$

where Δg is a specific Gibbs' energy of the material in bulk, V the nucleus' volume, σ the surface or interface energy, and S the nucleus' surface. Thus, ΔgV and σS are the terms corresponding to the volume and the surface of the phase, respectively. For a thermodynamically stable phase, $\Delta g < 0$, while the surface energy term is always positive.

For further discussion we make some assumptions, which are not essential for the problem but simplify the algebra. First, only a simple phase transformation of the type A′ → A″ will be modeled here. We consider a square-shaped nucleus on the flat substrate with height h and side d and neglect the density difference of the competitive phases. The two-dimensional lattices at the film−substrate interface are also considered to be squarelike with the lattice spacings a_s and a_f for the substrate and the film, respectively. The lattice mismatch is determined as $\epsilon = \Delta a/a_s = (a_f - a_s)/a_s$. Now we are ready to write the energy balance. First, we consider the case of the homogeneous lattice strain in the coherent film:

$$\Delta G'_f = \Delta g' d^2 h + \sigma_c^{i\prime} d^2 + \sigma^{v\prime}(d^2 + 4dh) + h\frac{\mu}{1-\nu}\epsilon^2 d^2 \quad (2)$$

$$\Delta G''_f = \Delta g'' d^2 h + \sigma_{ic}^{i\prime\prime} d^2 + \sigma^{v\prime\prime}(d^2 + 4dh) \quad (3)$$

The quantities Δg and σ have the same meaning as in eq 1. The index ′ refers to the nucleus of the phase growing epitaxially on the substrate and the index ″ refers to the nucleus of the incoherent phase. Indices "i" and "v" show the difference between the nucleus' interfaces with the substrate and vapor phase, indices "c" and "ic" denote the coherent and incoherent state of the interface, respectively, μ is a shear modulus, and ν is a Poisson ratio for the coherent phase. The epitaxial strain contribution disappears for the incoherent phase but for the cost of the essentially higher $\sigma^{i\prime\prime}$, as compared to that of $\sigma^{i\prime}$ (Table 1). We are especially interested in the case when $\Delta g''$ is more negative than $\Delta g'$. We assume in addition that $\sigma^{v\prime\prime} = \sigma^{v\prime}$. These assumptions restrict the class of objects we want to model here. Generally, the difference of $\sigma^{v\prime\prime}$ and $\sigma^{v\prime}$ can be even higher than the difference in the interface energies but it results in the growth, which is not controlled by the interface structure. Thus, we assume that the edges and surface of the island do not contribute to the difference of the free energies. Also, we do not consider the case when the second phase is able to form a semicoherent

Table 2. Survey of Literature Data on Epitaxial Stabilization Phenomena in Oxide Systems[a]

stable in bulk phase	epitaxial phase	substrates[b]	thickness, nm	technique	refs
TiO_2 (rutile)	TiO_2 (anatase)	(001)$SrTiO_3$, (001)$LaAlO_3$, (001)$La_{0.5}Sr_{0.5}CoO_3$, (001)MgO, (110)MgO	10−1000	MBE, MOCVD	50−55, 58
ZnO (wurtzite)	ZnO (zinc blend)	(001)ZnS || (001)GaAs	≤560	MOMBE	64
(Zn,Mg)O (wurtzite) + (Zn,Mg)O (rock salt) for $x > 0.04$	$Zn_{1-x}Mg_xO$ ($x \leq 0.36$, wurtzite)	(0001)Al_2O_3	≤500	MBE, PLD	78−81
(Zn,Mn)O (wurtzite) + (Zn,Mn)O (rock salt) for $x > 0.13$	$Zn_{1-x}Mn_xO$ ($x \leq 0.35$, wurtzite)	(0001)Al_2O_3	several 100s	PLD	82
Mn_3O_4 (tetragonal spinel−hausmanite)	Mn_3O_4 (cubic spinel)	(001)MgO	100	MOCVD	69
WO_3 (orthorhombic)	WO_3 (tetragonal)	$(1\bar{1}02)Al_2O_3$	30	EBE	73
α-Fe_2O_3	γ-Fe_2O_3	(001)MgO	100	MBE	74
$BaRuO_3$ (hexagonal, 9*R*-type)	$BaRuO_3$ (perovskite)	(001)$SrTiO_3$	100	RFS	90−93
—	$SrRu_{0.5}Sn_{0.5}O_3$ (perovskite)	(001)$KTaO_3$	600	PLD	94
$BaTi_{1-x}Nb_xO_3$ (perovskite)	$BaTi_{1-x}Nb_xO_3$ ($x = 0.01-0.15$) (hexagonal)	(0001)Al_2O_3	60	PLD	95
$RMnO_3$ (hexagonal)	$RMnO_3$ (R = Ho, Y, Tm, Lu) (perovskite)	(001)$LaAlO_3$, (001)$SrTiO_3$	100−200	MOCVD, PLD	99, 100
α-BaB_2O_4	β-BaB_2O_4	$(0\bar{0}01)Al_2O_3$, $(1\bar{1}02)Al_2O_3$	<500	PLD, MS, MOCVD	101−103
$BaCuO_2 + CuO$	$BaCu_3O_4$	(001)$LaAlO_3$, (001)$SrTiO_3$, (001)$RBa_2Cu_3O_7$	<300	MOCVD	109−113
$Nd_{1-x}MnO_3 + Mn_3O_4$	$NdMn_7O_{12}$	(001)$Nd_{1-x}MnO_3$	10	MOCVD	114
$BiFeO_3 + Bi_2Fe_4O_9$	$Bi_3Fe_5O_{12}$ (garnet)	(001)$Gd_3(Sc,Ga)_5O_{12}$, (111)$Gd_3(Sc,Ga)_5O_{12}$	<1000	RIBS, ECR and RFS, PLD	116−121
$BaO + BaRuO_3$	Ba_2RuO_4 (K_2NiF_4 type)	(001)$SrTiO_3$	150	PLD	123
Cr_2O_3 (corundum)	CrO_2 (rutile)	TiO_2 (rutile), (0001)Al_2O_3	1000	CVD	132−137
Mn_3O_4	MnO (rock salt)	(0001)Al_2O_3, (111)MgO	500	PLD	139
Fe_2O_3 (hematite)	Fe_3O_4 (spinel)	(001)MgO		MBE	142−144
Fe	Fe_3O_4 (spinel)	(001)MgO		MBE	142−144
Fe_2O_3 (hematite)	$Fe_{3-\delta}O_4$ ($0 < \delta \leq 0.33$) (spinel)	(001)MgO		MBE	75, 142−150
$Fe + Fe_3O_4$	$Fe_{1-x}O$ (rock salt)	(001)MgO		MBE	149
$R_2O_3 + NiO$	$RNiO_3$ (R = Pr, Nd, Sm, Gd) (perovskite)	(001)$LaAlO_3$, (001)$SrTiO_3$, (001)$RBa_2Cu_3O_7$	<400	MOCVD, PLD	156, 157
$La_2CuO_4 + CuO$	$LaCuO_{2.5}$ (orthorhombic)	(001)$SrTiO_3$	300	PLD	164

[a] Abbrevations: MOCVD, metal−organic chemical vapor deposition; MBE, molecular beam epitaxy; PLD, pulsed laser deposition; EBE, electron beam evaporation; RFS, radio frequency sputtering; MS, magnetron sputtering; RIBS, reactive ion beam sintering; ECR, electron cyclotron resonance. [b] Pseudocubic indices are used for some perovskite substrates.

interface instead of an incoherent one because of the diminishing of the interface energy difference and suppression of the epitaxial stabilization of the coherent phase.

One can also notice that equations would become more simple if we consider the bulk free energy per unit surface ($\Delta E_f = \Delta G_f/d^2$) instead of the bulk free energy ΔG_f and that ($\Delta E''_f - \Delta E'_f$) is a free energy per unit surface of the transformation from a coherent to incoherent phase ΔE:

$$\Delta E = h\left[(\Delta g'' - \Delta g') - \frac{\mu}{1-\nu}\epsilon^2\right] + (\sigma_{ic}^{i\,\prime\prime} - \sigma_c^{i\prime}) \quad (4)$$

This expression is a simple model of the epitaxial stabilization. In fact, the first member is always negative and the latter is always positive. The negative member increases linearly with the film thickness; the critical thickness value corresponds to $\Delta E = 0$. One can see that the lattice mismatch is an extremely important parameter: the transition energy is linearly dependent on free energy and surface energy differences, but its dependence upon the lattice mismatch is quadratic. If the lattice mismatch and free energy difference are both small, then the critical thickness of the epitaxially stabilized layer can be rather large. In particular, the values on the order of a few nanometers can be obtained

with the interface energies from Table 1 and free energy difference of 10 kJ/mol, which is a typical value for many solid-state reactions.

Now we proceed with more complex situations. In particular, for a thickness as large as that found in the last paragraph, the homogeneous strain in the film is no longer a good approximation. The strain relaxation by misfit dislocations introduces the inhomogeneous strain member and also changes the magnitude of the homogeneous strain. For simplicity, we set Burgers' vector equal to a_f. Then, the energy balance can be rewritten as follows:

$$\Delta E = h\left[(\Delta g'' - \Delta g') - \frac{\mu}{1-\nu}\left(\epsilon - \frac{a_f}{l}\right)^2\right] + (\sigma_{ic}^{i}{}'' - \sigma_c^{i}{}') - \frac{1}{l}\left(E_{core} + \frac{\mu}{1-\nu}Ka_f^2 \exp\left(-\frac{4\pi h}{l}\right)\right) \quad (5)$$

In this formula, l denotes the distance between neighboring misfit dislocations, E_{core} is a core energy of the misfit dislocation, and K is a numerical prefactor. In the limit case of a complete relaxation one obtains $l = a_f/\epsilon$ and the homogeneity strain member disappears. For $h > a_f/\epsilon$ the exponential member of the inhomogeneous strain disappears too and the thickness-independent part can be added to the interface energy, producing the interface energy of the semicoherent (sc) interface (see Table 1):

$$\Delta E = h(\Delta g'' - \Delta g') + (\sigma_{ic}^{i}{}'' - \sigma_{sc}^{i}{}') \quad (6)$$

Again, the latter member ($\sigma^{i}_{ic}{}'' - \sigma^{i}_{sc}{}'$) is positive and the first member is negative and is thickness-dependent. As compared to the case of the homogeneous strain, the ($\sigma_{ic}^{i}{}'' - \sigma_{sc}^{i}{}'$) member decreases due to the higher energy of the semicoherent interface as compared to that of the coherent one. But the first member decreases also due to the disappearance of the strain contribution. Thus, for the relaxed state we also obtain the conditions for the epitaxial stabilization. One can conclude that the lattice strain is not a necessary condition of the epitaxial stabilization in accordance with experimental findings discussed above. The result should not be confused with the relaxation in the metastable film when nucleation of the stable phase is prevented by kinetic barriers. In the latter case no critical thickness occurs. In contrast, the thermodynamic scenario demands a critical thickness, at which another, incoherent, phase starts to grow. This critical thickness is not directly related to the thickness of the pseudomorphic layer of Frank−Van der Merwe. Again, the quantitative estimations for the free energy difference of about 10 kJ/mol show that films of the thickness of a few nanometers can be stabilized.

As was mentioned above, there is another possibility of the strain relaxation, namely, the formation of periodic multiple-domain structures. This is especially important for the oxides, which can decrease their symmetry from the cubic one, like in the case of perovskites belonging to the *Pnma* space group. Here, no self-strain is necessary to transform the cubic perovskite to the low-symmetry one. Respectively, the Roitburd scenario[38] becomes a very effective strain relaxation mechanism. The homogeneous strain in the film is then decreased for the cost of the inhomogeneous strain in the substrate and domain walls in the film (we account for the energy contribution of these members in the same form as was done by Little and Zangwill[31]). If the relaxation by the mechanism is complete (as seems to be the case for epitaxially stabilized $RMnO_3$ perovskites, while the stable in bulk forms are hexagonal), then the energy balance takes the following form,

$$\Delta E = h(\Delta g'' - \Delta g') - K\epsilon^2\sqrt{h} + (\sigma_{ic}^{i}{}'' - \sigma_c^{i}{}') \quad (7)$$

where K is the material-related parameter. From the viewpoint of the epitaxial stabilization, this case can be preferable both for the strain relaxation by the misfit dislocations (by lower surface energy of the coherent interface) and for the homogeneous strain (by the lower increase of the ϵ^2 term with the film thickness).

Finally, one can note that the supposition that the incoherent phase forms a film free of any grain boundaries is quite unrealistic, as compared to the thin film growth experience. Usually, polycrystalline films with random orientation of the grains are observed. Polycrystallinity introduces the additional grain boundary or surface energy contribution, which we have neglected until now. In fact, in oxides the energy of the incoherent grain boundary interfaces can be rather large (the situation is not much different if the grains are separated from each other). With the mean grain size r (the edge of the squarelike grain) and mean grain boundary energy σ_{gb}'' we obtain another member, which is dependent on the film thickness (taking into account that the number of grains in the film is d^2/r^2 and $d \gg r$):

$$E_{gb} = \frac{2h\sigma_{gb}''}{r}, \text{ and respectively}$$

$$\Delta E = h\left[(\Delta g'' - \Delta g') + \frac{2\sigma_{gb}''}{r}\right] + (\sigma_{ic}^{i}{}'' - \sigma_{sc}^{i}{}') \quad (8)$$

The equation is quite different from those we have discussed above. First, because σ_{gb}'' for the random oriented material is of the same order of magnitude as σ_{ic}'', the new positive member must be quite large, as compared to other members. For islandlike polycrystalline growth we should substitute E_{gb} by $4h\sigma^{v}{}''/r$.

In fact, the coherent phase can also grow in an islandlike mode. In that case the term $4h\sigma^{v}{}'/r$ should be added to eq 8. If different in-plane orientations are allowed, then inhomogeneous strain in the substrate can be switched on, resulting in the hybridization of eqs 7 and 8. Respectively, the islandlike growth mode is not necessarily detrimental to epitaxial stabilization (see section III.A for an example).

Next, because of the linear dependence on the film thickness, huge values of the critical thickness or even absolute (thickness independent) stabilization can be obtained for very small r. The result is actually due to consideration of the grain size as a constant parameter of the thermodynamic model that is really not correct. The conditions of the true thermodynamic equilibrium correspond to the single-crystal film of the incoherent phase. The polycrystalline film is a metastable state. So, unexpectedly, we see that thermodynamic epitaxial stabilization can be dressed by an additional kinetic effect, which is not due to the metastable state of the

epitaxial film (as is supposed in the classical theories of the kinetic epitaxial stabilization), but because of the inevitably metastable state of the stable in bulk—but incoherent—phase.

Considering the grain size as a kinetic parameter, one should account for the thickness dependence of the grain size. The dependence is complex due to the different steps involved in the grain growth. Basically four steps can be considered: (1) independent growth of the nucleus ensemble (mass transfer between nuclei is allowed, but no contact of them); (2) interaction of nuclei (growth is retarded at the grain contacts; incoherent grain boundaries are formed); (3) reconstruction (incoherent grain boundaries are driven to be substituted by semicoherent ones, but pinning occurs at substrate surface defects); (4) later ripening (slow grain boundary diffusion is still present; stagnation occurs easily at surface grooves known as Mullins barriers). It is not sensible to incorporate all these steps in a simple model, so we consider only the first step (when $\sigma^{v\prime\prime}$ should be used instead of $\sigma_{gb}{}''$).

The thickness dependence of the grain size for the stationary growth of the polycrystalline island film is expected to follow $r \propto \sqrt{h}$ law (in-plane ripening results in $r^2 \propto t$ dependence following the Lifshits−Slezov approach and stationary growth implies $h \propto t$). Experimentally, $r \propto h^q$ ($0.3 < q < 0.9$) dependence was observed for different thin film materials.[165] One can see that it cuts off the possibility of the absolute stabilization, but allows still for the huge values of the critical thickness because the negative member increases only by a factor of $h^{(1-q)}$ in relation to the positive members, and not by a factor of h, as in the case of pure thermodynamic stabilization.

Definitely, this kinetic factor does not substitute the thermodynamic epitaxial stabilization. However, it seems to be difficult to find any case of the thermodynamic epitaxial stabilization, when this kinetic contribution can be canceled completely in the real vapor deposition experiment. Respectively, the experimentally found critical thickness of the epitaxial stabilization is expected to exceed the value calculated in the correct thermodynamic model.

Figure 11a presents a simple calculation of the energy change for the TiO_2(anatase) → TiO_2(rutile) transformation using eq 6 and eq 8. It is supposed that TiO_2-(anatase) grows epitaxially (e.g., on the (001)$LaAlO_3$ surface—see section IIa.A), forming a semicoherent interface with the substrate ($\sigma^{i}_{sc}{}' = 800$ mJ/m^2, Table 1). A hypothetical rutile film was supposed to form a high-energy incoherent interface with $\sigma^{i}_{ic}{}'' = 2500$ mJ/m^2, while the grain boundary energy $\sigma_{gb}{}''$ was taken to be 2500 mJ/m^2 as well. The $[\Delta g'' - \Delta g']$ term has been calculated from the known value of the free energy difference between rutile and anatase polymorphs, −5 kJ/mol.[47,48] The theoretical density values of 4.25 g/cm^3 for rutile and 3.89 g/cm^3 for anatase were used. Then, $[\Delta g'' - \Delta g']$ is equal to 243.7 J/cm^3. As can be seen from the figure, the epitaxial film of anatase is *thermodynamically stable* up to some critical thickness value corresponding to $\Delta E = 0$. If we suppose that the rutile film is formed by crystallites, whose size is equal to the square root of the film thickness (that is a quite realistic assumption), the critical thickness of the anatase film

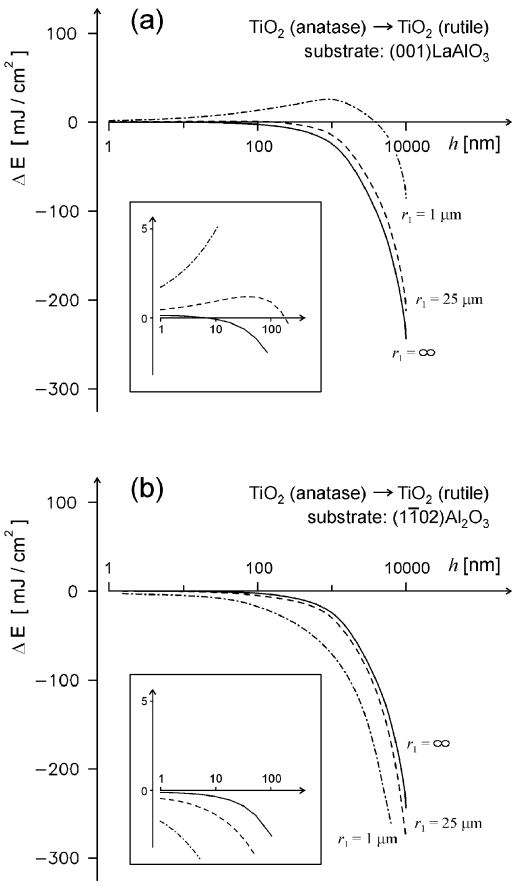

Figure 11. (a) Energy change for the transformation of TiO_2 anatase in 1 cm^2 of the epitaxial film on $LaAlO_3$ to rutile vs film thickness according to eq 6 (solid line) and eq 8. In the latter case, $r = \sqrt{hr_1}$ approximation has been used with $r_1 = 25\ \mu$m and $r_1 = 1\ \mu$m. Inset presents the enlarged dependence in the same coordinates. (b) The same for 1 cm^2 of TiO_2 film on $(1\bar{1}02)Al_2O_3$.

is somewhat above 4 μm! This result numerically approves the possibility of the thermodynamic epitaxial stabilization in relatively thick oxide films. Of course, often the situation is complicated by the presence of kinetic effects and the inherent loss of epitaxy in thick films. The opposite situation is illustrated by Figure 11b. In the case of TiO_2 growth on the $(1\bar{1}02)Al_2O_3$ surface, an epitaxial film of thermodynamically stable rutile polymorph is formed. Evidently, no driving force for anatase formation is present in this case, and ΔE for anatase to rutile conversion is negative for all values of the film thicknesses.

The model discussed above can be extended for more complex phase assemblies. However, this will not be done here because of the increasing complication of algebraic expressions without discovering any new aspects of the epitaxial stabilization.

VII. Conclusions

The experimental results and theoretical analysis allowed us to formulate the thermodynamic epitaxial stabilization as a drastic extension of the equilibrium $P-T-x$ stability field of the epitaxially grown phase due to the energy contribution from coherent and semicoherent film−substrate interfaces.

We have shown that the possibilities of the epitaxial stabilization in simple and complex oxides are much

broader than earlier theoretical estimations had supposed. In fact, one can speak about a new tool of solid state chemistry when a structure of interest can be constructed, even though it cannot be obtained as a bulk material. As well, many syntheses that need severe conditions in the bulk state (e.g., high pressure, highly oxidative environment, high temperature) can be realized in much more gentle conditions using this approach.

Here, the particular advantage of MOCVD technology over PVD techniques can be seen. MOCVD does not neeed a bulk target to prepare thin film material of the same composition and is at the same time a highly scalable industrial technology.[166] On the other hand, the sophisticated and highly expensive techniques such as MBE used to prepare homogeneously strained thin films are not exclusively necessary for epitaxial stabilization to occur, so far as the film strain is not a necessary condition of the epitaxial stabilization.

In conclusion, we propose the following criteria, which can be useful to distinguish experimentally the thermodynamic stabilization from stabilization for kinetic reasons:

1. *Zero strain optimum*. In contrast to kinetic stabilization, no strain is necessary to stabilize the epitaxial phase. Moreover, strain is a destructive factor for thermodynamic stabilization.

2. *Drastic mismatch effect (substrate effect).* The critical thickness of the stabilized layer decreases very rapidly with the increase of the lattice mismatch. It does not matter if the layer is strained or not.

3. *Strain relaxation invariance.* Relaxation of the strain both by misfit dislocations or by multiple-domain formation does not result in the loss of the stabilization effect.

4. *Relative compositional invariance (for multicomponent systems).* The appearance of stable in bulk secondary phases, along with an epitaxially stabilized phase, proves the equilibrium nature of the phenomenon.

5. *Growth rate and postannealing invariance.* So far as the stabilization was observed, no decrease of the deposition rate can make the phase disappear (but it can influence the critical thickness because of the kinetic dressing). Also, no postannealing under the growth conditions can produce any trace of the phase separation or spinodal decay. The effect of the growth rate in the case of the kinetic stabilization is just the opposite and postannealing usually influences the phase decomposition.

Considering the directions of further research of the epitaxial stabilization in oxide systems, we can outline that most of the information available concerns the deposition on the substrate surface with high symmetry (mostly, with square or hexagonal two-dimensional lattices). In fact, one can expect higher selectivity of the stabilization effect and more rich chemistry exploring the growth on the two-dimensional lattices with lower symmetry (rectangular, rectangular centered, or monoclinic). On the other hand, the strong dependence of the stabilization effect on the lattice mismatch allows for the possibility of the selective growth,[136,160,161] which can be very useful in microelectronic technology.

Acknowledgment. The authors would like to acknowledge INTAS−RFBR (Grant IR 97-1954) and VW Stiftung (Project I/73628) for financial support, A. A. Bosak, M. A. Novojilov, and A. A. Kamenev for undertaking part of the experimental work, and Prof. G. Wahl (IOPW, TU Braunschweig) and Prof. H. W. Zandbergen (National Centre for HREM, TU Delft) for fruitful cooperation during this study.

Addendum

The epitaxial stabilization of hexagonal $RMnO_3$ (R = Dy, Gd, Sm, Eu) phases on (111) $ZrO_2(Y_2O_3)$ was reported recently.[167] The bulk form of the materials is perovskite. The result should be compared to that described in section IIb.D. $RMnO_3$ phases (R = Ho, Tm, Lu), which are hexagonal in the bulk state, were stabilized in the perovskite form on the perovskite substrate. Thus, the stabilization effect is reversible and is controlled by the substrate structure.

References

(1) Sutton, A. P.; Balluffi, R. W. *Interfaces in Crystalline Materials*; Calendron Press: Oxford, 1995.
(2) Dankov, P. D. *Dokl. Akad. Nauk USSR* **1939**, *24*, 773 (in Russian).
(3) Dankov, P. D. *Zh. Fiz. Khim.* **1949**, *23*, 1025 (in Russian).
(4) Pashley, D. W. *Proc. Phys. Soc. London* **1951**, *65*, 33.
(5) Greene, J. E. *J. Vac. Sci. Technol. B* **1983**, *1*, 229.
(6) Farrow, R. F. C. *J. Vac. Sci. Technol. B* **1983**, *1*, 222.
(7) Grunthaner, F. J.; Madhukar, A. *J. Vac. Sci. Technol. B* **1983**, *1*, 462.
(8) Mahlin, E. S.; Chaudhari, P. In *Synthesis and Properties of Metastable Phases*; Mahlin, E. S., Rowland, T. J., Eds.; The Metallurgical Society of AIME: Warrendale, PA, 1980; p 11.
(9) Chopra, K. L. *Thin Film Phenomena*; McGraw-Hill Book Company: New York, 1969.
(10) Yang, M. H.; Flynn, C. P. *Phys. Rev. Lett.* **1989**, *62*, 2476.
(11) Flynn, C. P. *Phys. Rev. Lett.* **1986**, *57*, 599.
(12) Yang, M. H.; Flynn, C. P. *Phys. Rev. B* **1990**, *41*, 8500.
(13) Jesser, W. A. *Mater. Sci. Eng.* **1969**, *4*, 279.
(14) Quillec, M.; Launois, H.; Joncour, M. C. *J. Vac. Sci. Technol. B* **1983**, *1*, 238.
(15) Stringfellow, G. B. *J. Appl. Phys.* **1972**, *43*, 3455.
(16) Hirth, J. P.; Stringfellow, G. B. *J. Appl. Phys.* **1977**, *48*, 1813.
(17) Yang, J.; Amatatsu, Y.; Hashimoto, M.; Barna, A.; Barna, P. B. *Thin Solid Films* **2000**, *371*, 47.
(18) Wormeester, H.; Hüger, E.; Bauer, E. *Phys. Rev. Lett.* **1996**, *77*, 1540.
(19) Orton, J. W.; Foxon, C. T. *Rep. Prog. Phys.* **1998**, *61*, 1.
(20) Sun, X. L.; Yang, H.; Zheng, L. X.; Xu, D. P.; Li, J. B.; Wang, Y. T.; Li, G. H.; Wang, Z. G. *Appl. Phys. Lett.* **1999**, *74*, 2827.
(21) Lee, J. J.; Park, Y. S.; Yang, C. S.; Kim, H. S.; Kim, K. H.; Kang, K. Y.; Kang, T. W.; Park, S. H.; Lee, J. Y. *J. Cryst. Growth* **2000**, *213*, 33.
(22) Zhang, H.; Ye, Z.; Zhao, B. *J. Appl. Phys.* **2000**, *87*, 2830.
(23) Liu, H.; Chen, H.; Li, Z.; Wan, L.; Huang, Q.; Zhou, J.; Yang, N.; Tao, K.; Han, Y. J.; Luo, Y. *J. Cryst. Growth* **2000**, *212*, 391.
(24) Kim, I. W.; Li, Q.; Marks, L. D.; Barnett, S. A. *Appl. Phys. Lett.* **2001**, *78*, 892.
(25) Madan, A.; Kim, I. W.; Cheng, S. C.; Yashar, P.; Dravid, V. P.; Barnett, S. A. *Phys. Rev. Lett.* **1997**, *78*, 1743.
(26) Lin, W.-T.; Meng, L.-C.; Chen, G.-J.; Liu, H.-S. *Appl. Phys. Lett.* **1995**, *66*, 2066.
(27) Shin, C.-S.; Gall, D.; Desjardins, P.; Vailionis, A.; Kim, H.; Petrov, I.; Greene, J. E.; Oden, M. *Appl. Phys. Lett.* **1999**, *75*, 3808.
(28) Yashar, P.; Chu, X.; Barnett, S. A.; Rechner, J.; Wang, Y. Y.; Wong, M. S.; Sproul, W. D. *Appl. Phys. Lett.* **1998**, *72*, 987.
(29) Umeya, H.; Kitamura, K.; Jia, A.; Shimotomai, M.; Kato, Y.; Kobayashi, M.; Yoshikawa, A.; Takahashi, K. *J. Cryst. Growth* **2000**, *214/215*, 192.
(30) Szczerbakow, A.; Bak-Misiuk, J.; Dynowska, E.; Ghali, M.; Godlewski, M.; Ivanov, V. Yu.; Swiatek, K. *J. Cryst. Growth* **2000**, *216*, 532.
(31) Little, S.; Zangwill, A. *Phys. Rev. B* **1994**, *49*, 16659.
(32) Bruinsma, R.; Zangwill, A. *J. Phys.* **1986**, *47*, 2055.
(33) Bruinsma, R.; Zangwill, A. *Europhys. Lett.* **1987**, *4*, 729.
(34) Wood, D. M.; Zunger, A. *Phys. Rev. B* **1989**, *40*, 4062.
(35) Zunger, A. In *Handbook of Crystal Growth*; Hurle, D. T. J., Ed.; Elsevier: Amsterdam, 1994; Vol. 3, p 997.
(36) Zunger, A.; Wood, D. M. *J. Cryst. Growth* **1989**, *98*, 1.
(37) Little, S.; Zangwill, A. *Phys. Rev. B* **1992**, *46*, 7981.
(38) Roitburd, A. L. *Phys. Status Solidi A* **1976**, *37*, 329.

(39) Bozovic, I.; Eckstein, J. N. In *Physics of High-Temperature Superconductors*, 5; Ginsberg, D., Ed.; World Scientific: River Edge, NJ, 1996.
(40) Verbist, K.; Milat, O.; Van Tendeloo, G.; Arrouy, F.; Williams, E. J.; Rossel, C.; Mächler, E.; Locquet, J.-P. *Phys. Rev. B* **1997**, *56*, 853.
(41) Balestrino, G.; Martellucci, S.; Medaglia, P. G.; Paoletti A.; Petrocelli, G. *Physica C* **1998**, *302*, 78.
(42) Yamamoto, H.; Naito, M.; Sato, H. *Physica C* **2000**, *338*, 29.
(43) Mercey, B.; Salvador, P. A.; Prellier, W.; Doan, T.-D.; Wolfman, J.; Hamet, J.-F.; Hervieu, M.; Raveau, B. *J. Mater. Chem.* **1999**, *9*, 233.
(44) Sambi, M.; Sangiovanni, G.; Granozzi, G.; Parmigiani, F. *Phys. Rev. B* **1997**, *55*, 7850.
(45) Gota, S.; Guiot, E.; Henriot, M.; Gautier-Soyer, M. *Phys. Rev. B* **1999**, *60*, 14387.
(46) Clarke, D. R. *Phys. Status Solidi A* **1998**, *166*, 183.
(47) Barin, I. *Thermochemical Data of Pure Substances*, Pt. 2; VCH: Weinheim, 1989.
(48) *Handbook of Chemistry and Physics*; West, R. C., Ed.; CRC: Cleveland, 1986.
(49) *The Oxide Handbook*; Samsonov, G. V., Ed.; IFI/Plenum Data Company: New York, 1982; in Russian: *Fiziko-Khimicheskie Svoistva Okislov*; Samsonov, G. V., Ed.; Metalurgiya: Moscow, 1978.
(50) Chen, S.; Mason, M. G.; Gysling, H. J.; Paz-Pujalt, G. R.; Blanton, T. N.; Castro, T.; Chen, K. M.; Fictorie, C. P.; Gladfelter, W. L.; Franciosi, A.; Cohen, P. I.; Evans, J. F. *J. Vac. Sci. Technol. A* **1993**, *11*, 2419.
(51) Tokita, S.; Tanaka, N.; Saitoh, H. *Jpn. J. Appl. Phys.* **2000**, *39*, L169.
(52) Herman, G. S.; Gao, Y. *Thin Solid Films* **2001**, *397*, 157.
(53) Sugimura, W.; Yamazaki, A.; Shigetani, H.; Tanaka, J.; Mitsuhashi, T. *Jpn. J. Appl. Phys.* **1997**, *36*, 7358.
(54) Murakami, M.; Matsumoto, Y.; Nakajima, K.; Makino, T.; Segawa, Y.; Chikyow, T.; Ahmet, P.; Kawasaki, M.; Koinuma, H. *Appl. Phys. Lett.* **2001**, *78*, 2664.
(55) Park, B. H.; Li, L. S.; Gibbons, B. J.; Huang, J. Y.; Jia, Q. X. *Appl. Phys. Lett.* **2001**, *79*, 2797.
(56) Gao, Y.; Thevuthasan, S.; McCready, D. E.; Engelhard, M. *J. Cryst. Growth* **2000**, *212*, 178.
(57) Schuisky, M.; Hårsta, A. *J. Phys. IV France* **1999**, *9*, 381.
(58) Bosak, A. A.; Botev, A. N.; Gorbenko, O. Yu.; Graboy, I. E.; Samoilenkov, S. V.; Kaul, A. R.; Dubourdieu, C.; Senateur, J. P. *J. Phys. IV France* **2001**, *11*, 93.
(59) Millon, E.; Albert, O.; Loulergue, J. C.; Etchepare, J.; Hulin, D.; Seiler, W.; Perriere, J. *J. Appl. Phys.* **2000**, *88*, 6937.
(60) Ryu, Y. R.; Zhu, S.; Budai, J. D.; Chandrasekhar, H. R.; Miceli, P. F.; White, H. W. *J. Appl. Phys.* **2000**, *88*, 201.
(61) Gorla, C. R.; Emanetoglu, N. W.; Liang, S.; Mayo, W. E.; Lu, Y.; Wraback, M.; Shen, H. *J. Appl. Phys.* **1999**, *85*, 2595.
(62) Kim, T. W.; Yoon, Y. S *J. Cryst. Growth* **2000**, *212*, 411.
(63) Chen, Y.; Hong, S.; Ko, H.; Nakajima, M.; Yao, T.; Segawa, Y. *Appl. Phys. Lett.* **2000**, *76*, 245.
(64) Ashrafi, A. B. M. A.; Ueta, A.; Avramescu, A.; Kumano, H.; Suemune, I.; Ok, Y.-W.; Seong, T.-Y. *Appl. Phys. Lett.* **2000**, *76*, 550.
(65) Jaffe, E.; Hess, A. C. *Phys. Rev. B* **1993**, *48*, 7903.
(66) Tromel, G.; Fix, W.; Koch, K.; Schaberg, F. *Erzmetall* **1976**, *29*, 234.
(67) Guo, L. W.; Peng, D. L.; Makino, H.; Inaba, K.; Ko, H. J.; Sumiyama, K.; Yao, T. *J. Magn. Magn. Mater.* **2000**, *213*, 321.
(68) Guo, L. W.; Ko, H. J.; Makino, H.; Chen, Y. F.; Inaba, K.; Yao, T. *J. Cryst. Growth* **1999**, *205*, 531.
(69) Gorbenko, O. Yu.; Graboy, I. E.; Amelichev, V. A.; Bosak, A. A.; Kaul, A. R.; Guettler, B.; Svetchnikov, V. L.; Zandbergen, H. W. *Solid State Commun.* **2002**, in press.
(70) Woodward, P.; Sleight, A.; Vogt, T. *J. Phys. Chem. Solids* **1995**, *56*, 1305.
(71) Salje, E. *Acta Crystallogr. B* **1977**, *33*, 574.
(72) Kehl, W.; Hay, R.; Wahl, D. *J. Appl. Phys.* **1952**, *23*, 212.
(73) LeGore, L. J.; Greenwood, O. D.; Paulus, J. W.; Frankel, D. J.; Lad, R. J. *J. Vac. Sci. Technol. A* **1997**, *15*, 1223.
(74) Gao, Y.; Kim, Y. J.; Thevuthasan, S.; Chambers, S. A.; Lubitz, P. *J. Appl. Phys.* **1997**, *81*, 3253.
(75) Gao, Y.; Kim, Y. J.; Chambers, S. A.; Bai, G. *J. Vac. Sci. Technol. A* **1997**, *15*, 332.
(76) Sarver, J. F.; Katnack, F. L.; Hummel, F. A. *J. Electrochem. Soc.* **1959**, *106*, 960.
(77) Bates, C. H.; White, W. B.; Roy, R. *J. Inorg. Nucl. Chem.* **1966**, *28*, 397.
(78) Ohtomo, A.; Kawasaki, M.; Koida, T.; Masubuchi, M.; Koinuma, H.; Sakurai, Y.; Yoshida, Y.; Yasuda, T.; Segawa, Y. *Appl. Phys. Lett.* **1998**, *72*, 2466.
(79) Matsumoto, Y.; Murakami, M.; Jin, Z. W.; Ohtomo, A.; Lipmaa, M.; Kawasaki, M.; Koinuma, H. *Jpn. J. Appl. Phys.* **1999**, *68*, L603.
(80) Ohtomo, A.; Shiroki, R.; Ohkubo, I.; Koinuma, H.; Kawasaki, M. *Appl. Phys. Lett.* **1999**, *75*, 4088.
(81) Sharma, A. K.; Narayan, J.; Muth, J. F.; Teng, C. W.; Jin, C.; Kvit, A.; Kolbas, R. M.; Holland, O. W. *Appl. Phys. Lett.* **1999**, *75*, 3327.
(82) Fukumura, T.; Jin, Z.; Ohtomo, A.; Koinuma, H.; Kawasaki, M. *Appl. Phys. Lett.* **1999**, *75*, 3366.
(83) Randall, J. J.; Ward, R. *J. Am. Chem. Soc.* **1959**, *81*, 2629.
(84) Donohue, P. C.; Katz, L.; Ward, R. *Inorg. Chem.* **1965**, *4*, 306.
(85) Hong, S. T.; Sleight, A. W. *J. Solid State Chem.* **1997**, *128*, 251.
(86) Longo, J. M.; Kafalas, J. A. *Mater. Res. Bull.* **1968**, *3*, 687.
(87) Lee, M. K.; Eom, C. B.; Tian, W.; Pan, X. Q.; Smoak, M. C.; Tsui, F.; Krajewski, J. J. *Appl. Phys. Lett.* **2000**, *77*, 364.
(88) Tian, W.; Pan, X. Q.; Lee, M. K.; Eom, C. B. *Appl. Phys. Lett.* **2000**, *77*, 1985.
(89) Lee, M. K.; Eom, C. B.; Lettieri, J.; Scrymgeour, I. W.; Schlom, D. G.; Tian, W.; Pan, X. Q.; Ryan, P. A.; Tsui, F. *Appl. Phys. Lett.* **2001**, *78*, 329.
(90) Fukushima, N.; Sano, K.; Schimutzu, T.; Abe, K.; Komatsu, S. *Appl. Phys. Lett.* **1998**, *73*, 1200.
(91) Fukushima, N.; Sano, K.; Schimutzu, T.; Abe, K.; Komatsu, S. *Mater. Res. Soc. Symp. Proc.* **1998**, *494*, 35.
(92) Lettieri, J.; Scrymgeour, I. W.; Schlom, D. G.; Lee, M. K.; Eom, C. B. *Appl. Phys. Lett.* **2000**, *77*, 600.
(93) Fukushima, N.; Sano, K.; Schimizu, T.; Abe, K.; Komatsu, S.; Takeno, S. *Appl. Phys. Lett.* **2000**, *77*, 602.
(94) Christen, H.-M.; Boatner, L. A.; Budai, J. D.; Chisholm, M. F.; Gea, L. A.; Norton, D. P.; Gerber, C. *Appl. Phys. Lett.* **1997**, *70*, 2147.
(95) Khan, M. N.; Kim, H.-T.; Kusawake, T.; Kudo, H.; Ohshima, K.; Uwe, H. *J. Appl. Phys.* **1999**, *86*, 2307.
(96) Yakel, H. L.; Kohler, W. C.; Bertaut, E. F.; Forrat, E. F. *Acta Crystallogr.* **1963**, *16*, 957.
(97) Waintal, A.; Chenavas, J. *Mater. Res. Bull.* **1967**, *2*, 819.
(98) Szabo, G. Thèse University of Lyon, Lyon, France, 1969.
(99) Bosak, A. A.; Kamenev, A. A.; Graboy, I. E.; Antonov, S. V.; Gorbenko, O. Yu.; Kaul, A. R.; Dubourdieu, C.; Senateur, J. P.; Svechnikov, V. L.; Zandbergen, H. W.; Hollaender, B. *Thin Solid Films* **2001**, *400*, 149.
(100) Salvador, P. A.; Doan, T. D.; Mercey, B.; Raveau, B. *Chem. Mater.* **1998**, *10*, 2592.
(101) Liao, H. B.; Xiao, R. F.; Yu, P.; Wong, G. K. L.; Zheng, J. Q. *J. Vac. Sci. Technol. A* **1996**, *14*, 2651.
(102) Xiao, R.-F.; Ng, L. C.; Yu. P.; Wong, G. K. L. *Appl. Phys. Lett.* **1995**, *67*, 305.
(103) Studebaker, D. B.; Stauf, G. T.; Baum, T. H.; Marks, T. J.; Zhou, H.; Wong, G. K. *Appl. Phys. Lett.* **1997**, *70*, 565.
(104) Voronin, G. F.; Degterov, S. A. *J. Solid State Chem.* **1994**, *110*, 50, and references therein.
(105) Lindemer, T. B.; Specht, E. D. *Physica C* **1995**, *255*, 81, and references therein.
(106) Bertinotti, A.; Hamman, J.; Luzet, D.; Vincent, E. *Physica C* **1989**, *160*, 227.
(107) Takano, M.; Takeda, Y.; Okada, H.; Miyamoto, M.; Kusaka, K. *Physica C* **1989**, *159*, 375.
(108) Hiroi, Z.; Azuma, M.; Takano, M.; Bando, Y. *J. Solid State Chem.* **1991**, *95*, 230.
(109) Samoylenkov, S. V.; Gorbenko, O. Yu.; Graboy, I. E.; Kaul, A. R.; Zandbergen, H. W.; Connolly, E. *Chem. Mater.* **1999**, *11*, 2417.
(110) Güttler, B.; Samoylenkov, S. V.; Gorbenko, O. Yu. *Physica C* **1999**, *324*, 123.
(111) Zandbergen, H. W.; Jansen, J.; Svetchnikov, V. L.; Graboy, I. E.; Samoylenkov, S. V.; Gorbenko, O. Yu.; Kaul, A. R. *Physica C* **1999**, *328*, 211.
(112) Samoilenkov, S. V.; Gorbenko, O. Yu.; Papucha, S. V.; Mirin, N. A.; Graboy, I. E.; Kaul, A. R.; Stadel, O.; Wahl, G.; Zandbergen, H. W. *IOP Conf. Ser.* **2000**, *167* (v.2), 125.
(113) Kaul, A. R.; Gorbenko, O. Yu.; Graboy, I. E.; Samoilenkov, S. V.; Novojilov, M. A.; Bosak, A. A.; Zandbergen, H. W.; Wahl, G. *Int. J. Inorg. Mater.* **2001**, *3*, 1177.
(114) Bosak, A. A.; Gorbenko, O. Yu.; Kaul, A. R.; Graboy, I. E.; Dubourdieu, C.; Senateur, J. P.; Zandbergen, H. W. *J. Magn. Magn. Mater.* **2000**, *211*, 61.
(115) Bochu, B.; Chenavas, J.; Joubert, J. C.; Marezio, M. *J. Solid State Chem.* **1974**, *11*, 88.
(116) Adachi, N.; Denysenkov, V. P.; Khartsev, S. I.; Grishin, A. M.; Okuda, T. *J. Appl. Phys.* **2000**, *88*, 2734.
(117) Okuda, T.; Katayama, T.; Kobayashi, H.; Kobayashi, N. *J. Appl. Phys.* **1990**, *67*, 4944.
(118) Thavendrarajah, A.; Pardavi-Horvath, M.; Wigen, P. E.; Gomi, M. *IEEE Trans. Magn.* **1989**, *25*, 4015.
(119) Mino, S.; Matsuoka, M.; Tate, A.; Shibukawa, A.; Ono, K. *Jpn. J. Appl. Phys.* **1992**, *31*, 1786.
(120) Chern, M. Y.; Liaw, J. S. *Jpn. J. Appl. Phys.* **1997**, *36*, 1049.
(121) Watanabe, N.; Takahashi, N.; Tsushima, K. *Mater. Chem. Phys.* **1998**, *54*, 173.
(122) Kafalas, J. A.; Longo, J. M. *J. Solid State Chem.* **1972**, *4*, 55.
(123) Jia, Y.; Zurbuchen, M. A.; Wozniak, S.; Carim, A. H.; Schlom, D. G.; Zou, L.-N.; Briczinski, S.; Liu, Y. *Appl. Phys. Lett.* **1999**, *74*, 3830.

(124) Selinder, T. I.; Helmersson, U.; Han, Z.; Sundgren, J.-E.; Sjöström, H.; Wallenberg, L. R. *Physica C* **1992**, *202*, 69.
(125) Dorignac, D.; Schamm, S.; Grigis, C.; Sévely, J.; Santisto, J.; Figueras, A. *Physica C* **1994**, *235*−*240*, 617.
(126) Verbist, K.; Vasiliev, A. L.; van Tendeloo, G. *Appl. Phys. Lett.* **1995**, *66*, 1424.
(127) Selinder, T. I.; Helmersson, U.; Han, Z.; Wallenberg, L. R. *Thin Solid Films* **1993**, *229*, 237.
(128) Scotti di Uccio, U.; Miletto Granozio, F.; Di Chiara, A.; Tafuri, F.; Lebedev, O. I.; Verbist, K.; van Tendeloo, G. *Physica C* **1999**, *321*, 162.
(129) Meng, G.; Zhou, G.; Schneider, R.; Sarma, B. K.; Levy, M. *Physica C* **1993**, *214*, 297.
(130) Ranno, L.; Barry, A.; Coey, J. M. D. *J. Appl. Phys.* **1997**, *81*, 5774.
(131) *Binary Alloy Phase Diagrams*, 2nd ed; Okamoto, H., Subramanian, P. R., Kacprzak, L., Eds.; ASM International: Materials Park, OH, 1990; Vol. 2.
(132) Ivanov, P. G.; Watts, S. M.; Lind, D. M. *J. Appl. Phys.* **2001**, *89*, 1035.
(133) Yang, F. Y.; Chien, C. L.; Ferrari, E. F.; Li, X. W.; Xiao, G.; Gupta, A. *Appl. Phys. Lett.* **2000**, *77*, 286.
(134) Li, X. W.; Gupta, A.; McGuire, T. R.; Duncombe, P. R.; Xiao, G. *J. Appl. Phys.* **1999**, *85*, 5585.
(135) Li, X. W.; Gupta, A.; Xiao, G. *Appl. Phys. Lett.* **1999**, *75*, 713.
(136) Gupta, A.; Li, X. W.; Guha, S.; Xiao, G. *Appl. Phys. Lett.* **1999**, *75*, 2996.
(137) Suzuki, K.; Tedrow, P. M. *Solid State Commun.* **1998**, *107*, 583.
(138) Egdell, R. G.; Brand, E.; Kellett, D. *J. Mater. Chem.* **1999**, *9*, 2717.
(139) Neubeck, W.; Ranno, L.; Hunt, M. B.; Vettier, C.; Givord, D. *Appl Surf. Sci.* **1999**, *138/139*, 195.
(140) Langell, M. A.; Hutchings, C. W.; Carson, G. A.; Nassir, M. H. *J. Vac. Sci. Technol. A* **1996**, *14*, 1656.
(141) Darken, L. S.; Curry, R. W. *J. Am. Ceram. Soc.* **1946**, *67*, 1398; **1946**, *68*, 798.
(142) Fujii, T.; Takano, M.; Katano, R.; Bando, Y.; Isozumi, Y. *J. Appl. Phys.* **1989**, *66*, 3168.
(143) Fujii, T.; Takano, M.; Katano, R.; Bando, Y.; Isozumi, Y. *J. Cryst. Growth* **1990**, *99*, 606.
(144) Takano, M.; Fujii, T.; Bando, Y. In *New Functionality Materials, C, Synthetic Process and Control of Functionality Materials*; Tsuruta, T., Doyama, M., Seno, M., Eds.; Elsevier Science Pub. BV: North-Holland, 1993; p 745.
(145) Lind, D. M.; Berry, S. D.; Chern, G.; Mathias, H.; Testardi, L. R. *J. Appl. Phys.* **1991**, *70*, 6218.
(146) Lind, D. M.; Berry, S. D.; Chern, G.; Mathias, H.; Testardi, L. R. *Phys. Rev. B* **1992**, *45*, 1838.
(147) Lind, D. M.; Tay, S. P.; Berry, S. D.; Borchers, J. A.; Erwin, R. W. *J. Appl. Phys.* **1993**, *73*, 6886.
(148) Voogt, F. C.; Hibma, T.; Smulders, P. J. M.; Nielsen, L. *J. Cryst. Growth* **1997**, *174*, 440.
(149) Gao, Y.; Kim, Y. J.; Chambers, S. A. *J. Mater. Res.* **1998**, *13*, 2003.
(150) Voogt, F. C.; Fujii, T.; Smulders, P. J. M.; Niesen, L.; James, M. A.; Hibma, T. *Phys. Rev B* **1999**, *60*, 11193.
(151) Barbieri, A.; Weiss, W.; van Hove, M. A.; Samorjai, G. A. *Surf. Sci.* **1994**, *302*, 259.
(152) Kurtz, R. L.; Karunamuni, J.; Stockbauer, R. L. *Phys. Rev. B* **1999**, *60*, 16342.
(153) Kim, H. J.; Park, J. H.; Vescovo, E. *Phys. Rev B* **2000**, *61*, 15284.
(154) Chang, C. L.; Chern, G.; Chen, C. L.; Hsieh, H. H.; Dong, C. L.; Pong, W. F.; Chao, C. H.; Chien, H. C.; Chang, S. L. *Solid State Commun.* **1999**, *109*, 599.
(155) Lacorre, P.; Torrance, J. B.; Pannetier, J.; Nazzal, A. I.; Wang, P. W.; Huang, T. C. *J. Solid State Chem.* **1991**, *91*, 225.
(156) Novojilov, M. A.; Gorbenko, O. Yu.; Graboy, I. E.; Kaul, A. R.; Zandbergen, H. W.; Babushkina, N. A.; Belova, L. M. *Appl. Phys. Lett.* **2000**, *76*, 2041.
(157) Catalan, G.; Bowman, R. M.; Gregg, J. M. *J. Appl. Phys.* **2000**, *87*, 606.
(158) Kanke, Y.; Navrotsky, A. *J. Solid State Chem.* **1998**, *141*, 424.
(159) Gorbenko, O. Yu.; Novozhilov, M. A.; Graboy, I. E.; Amelichev, V. A.; Bosak, A. A.; Kaul, A. R.; Guettler, B.; Wahl, G.; Babushkina, N. A.; Belova, L. M.; Zandbergen, H. W. *Int. J. Inorg. Mater.* **2001**, *3*, 1303.
(160) Gorbenko, O. Yu.; Graboy, I. E.; Novozhilov, M. A.; Kaul, A. R.; Wahl, G.; Svetchnikov, V. L. *J. Phys. IV France* **2001**, *11*, Pr3−247.
(161) Novojilov, M. A.; Gorbenko, O. Yu.; Nikulin, I. V.; Graboy, I. E.; Kaul, A. R.; Babushkina, N. A.; Belova, L. M. *Int. J. Inorg. Mater.* **2001**, *3*, 1165.
(162) Karppinen, M.; Yamauchi, H.; Suematsu, H.; Isawa, K.; Nagano, M.; Itti, R.; Fukunaga, O. *J. Solid State Chem.* **1997**, *130*, 213.
(163) Hiroi, Z.; Takano, M. *Nature* **1995**, *377*, 41.
(164) Gupta, A.; Hussey, B. W.; Guloy, A. M.; Shaw, T. M.; Saraf, R. F.; Bringley, J. F.; Scott, B. A. *J. Solid State Chem.* **1994**, *108*, 202.
(165) Ievlev, V. M.; Bugakov, A. V.; Trophimov, V. I. *Growth and substructure of condensed films*; VGTU: Voronezh, 2000; p 50 (in Russian).
(166) *CVD of Nonmetals*; Rees, W. S., Jr., Ed.; Wiley-VCH: Weinheim, 1996.
(167) Bosak, A. A.; Dubourdieu, C.; Senateur, J. P.; Gorbenko, O. Yu.; Kaul, A. R. *J. Mater. Chem.* **2002**, *12*, 800.

CM021111V